

1415 N CHERRY AVE
CHICAGO, IL 60642
(312) 281-6900
DMDII.ORG
DMDII@UILABS.ORG



DMDII
+ a UI LABS Collaboration

DIGITIZING AMERICAN MANUFACTURING

DMDII FINAL PROJECT REPORT

ADAPTIVE MACHINING TOOLKIT

Principle Investigator / Email Address	Dean Robinson, robinsonm@ge.com
Project Team Lead	General Electric Company (GE) acting through GE Global Research
Project Designation	DMDII-14-07-01
UI LABS Contract Number	0220160011
Project Participants	University of Wisconsin Madison, Metrologic Group, Western Illinois University/Quad City Manufacturing Lab, Genesis System Group
DMDII Funding Value	\$950,238
Project Team Cost Share	\$950,239
Award Date	June 15, 2016
Completion Date	July 31, 2018

SPONSORSHIP DISCLAIMER STATEMENT: This project was completed under the Cooperative Agreement W31P4Q-14-2-0001, between U.S. Army - Army Contracting Command - Redstone and UI LABS on behalf of the Digital Manufacturing and Design Innovation Institute. Any opinions, findings, and conclusions or recommendations expressed in this material are those of the author(s) and do not necessarily reflect the views of the Department of the Army.

DISTRIBUTION STATEMENT A. Approved for public release; distribution unlimited.

TABLE OF CONTENTS

Page(s)	Section
	I. Executive Summary (1-2 pages)
	II. Project Overview
	III. KPI's & Metrics
	IV. Technology Outcomes
	V. Accessing the Technology
	VI. Industry Impact & Potential
	VII. Tech Transition Plan & Commercialization
	VIII. Workforce Development
	IX. Conclusions/Recommendations
	X. Lessons Learned
	XI. Definitions
	XII. Appendices

I EXECUTIVE SUMMARY

I.1 OVERVIEW

Geometric-adaptive machining (GAM) technology allows machine tools or robots to accommodate and adjust to variations in workpiece geometry and/or position. While it is possible to find commercially-available geometric-adaptive solutions today, existing solutions require highly expensive and time-consuming development of custom software and/or hardware, which is specific to both incoming part geometry and the computer numerical control (CNC) controller. Further, implementation efforts require a means to ingest input data from non-contact or touch-probe metrology systems and align that data to the coordinate system of the part and the machine tool. These difficulties limit the ability of small and medium sized enterprises (SMEs) to adopt geometric-adaptive machining solutions in their operations, which could impact their global competitiveness.

To overcome these challenges, we developed a plug-and-play hardware and software toolkit solution that enable legacy and modern CNC machine tools and robots to perform geometric-adaptive-machining. The idea of the plug-and-play geometric adaptive machining solution is to enable CNC machine tools and robots to be retrofitted with the capability to perform adaptive machining. The challenge was to develop a plug-and-play solution that satisfies the many different adaptive machining scenarios that exist. To solve this problem, the adaptive machining toolkit was developed as modules wrapped using macros and integrated into a commercial inspection software, Metrolog. The Metrolog software provides a workflow-oriented way of deploying geometric-adaptive machining solution for CNC machine tools and robots.

I.2 KEY TECHNOLOGY INNOVATIONS

Key technical accomplishments of this program were the development and integration of all the key modules necessary for a plug and play CNC machine tool and robot toolkit. These modules include CAD neutral algorithm for 3-D best-fitting, CNC machine G-code morphing, Robot LS file morphing, and technique for selecting probe points touch probe. The following key technology innovations were developed and integrated into the toolkit:

Integration of Non-contact In-situ Measurement - Techniques for using commercially available non-contact metrology hardware to measure part or workpiece in-situ without the need for custom fixtures or software. Algorithms that automate segmenting and applying 3-D alignment to large data set when non-contact metrology is employed to measure part geometry.

Point Selection for On-Machine Probing - One of the key decisions for a successful adaptive machining application development is a choice of robust, accessible measurement points to compute the distortion map. In common practice, this requires a computational geometry expert to choose probe points that adequately reflect the actual geometry of the part. In this program, the University of Wisconsin-Madison developed algorithms to automate the selection and optimization of the probe points. These algorithms select probe points based on nominal part geometry and expected part variation, thereby eliminating erroneous modes of surface fitting.

Toolpath Morphing - State-of-the-art 3-D geometry “multi-level b-spline morphing” technique that enable complex 3-D geometry variations to be accurately and smoothly modeled for machining. Algorithms that accurately apply part or workpiece variations to modify toolpath program at the G-code level for CNC adaptive machining and robot commands level for robotic adaptive machining

Modular Software Architecture - The geometric-adaptive machining toolkit is designed to be modular and is executed as a workflow in Metrolog inspection software. This allow users to chain together different algorithms to select their toolpath adaptation strategy. For example, if user is doing adaptive machining for milling, user can choose workflow template and the sequence of operations are easily controlled though Metrolog user interface.

CAD Neutral Platform - To enable a complete stand-alone solution, Parasolid geometric kernel was chosen as the CAD kernel. Parasolid geometric kernel enable users to use their CAD platform of choice to define nominal geometry.

1.3 PROJECT OUTCOMES AND RECOMMENDATIONS

The outcome of the effort is a smart plug-and-play, user friendly and hardware and software toolkit that enables legacy or modern CNC machine tools and robots to perform geometric adaptive machining (GAM) to accommodate variation in the incoming part geometry. The toolkit contains CAD agnostic morphing algorithms that reconcile the difference between nominal and actual workpiece, and provide real-time modification of tool paths that can run on any machine tool or robot controller. The toolkit is compatible with data generated from both contact and non-contact measurement systems. The software is architected to be modular with the ability to chain various pieces of software to quickly develop and deploy an adaptive machining solution.

The toolkit was used to successfully demonstrate geometric adaptive machining for both CNC machine tools and robots. Demonstrations of GAM for robotic applications were successfully carried out on two use cases: an adaptor arm casting and a sheet metal casting tree. The adaptor arm casting was provided by the Rock Island Arsenal (RIA) and is a component that the RIA currently manufactures. The sheet metal casting tree was fabricated from sheet metal to facilitate cutting with a plasma torch. The morphed tool paths in both cases were accurately located relative to the parts. Using the GAM toolkit reduced the time to cut the adaptor arm by more than 50% of production data provided by the RIA. Demonstrations of the GAM for CNC machine tool applications were carried out on three use cases: an airfoil shape artifact, an impeller, and a swivel link. The airfoil shape artifact was intentionally deformed, and the GAM toolkit generated morphed toolpaths programs that were used produces tip shelf feature within tolerance. The impeller was produced via powder bed fusion and using GAM toolkit successfully captures part variation and produced toolpath used to remove the support material. Three out-of-tolerance swivel link prototypes were milled from aluminum blocks. The GAM toolkit was able center the milled features to the existing casting within 0.20 mm (0.008”) or less. The accuracy achieved satisfies the requirements of the RIA, ensuring full strength parts.

The key design innovation of this program was the development of a “plug and play” GAM toolkit that links what was previously been isolated solutions for geometric-adaptive machining into a single software platform that is computer-aided design (CAD) system and machine tool agnostic. This will eliminate the expense associated with development of custom software and/or hardware for each new application of geometric adaptive machining and will reduce the development time for a typical adaptive machining application by over 10X (from 3-6 months to 1 week). The toolkit can work across a wide range of applications and controllers for both CNC machine tools and robots

II PROJECT REVIEW

II.1 PROJECT OBJECTIVES

A team led by GE Global Research (GE) proposes to develop a revolutionary new plug-and-play hardware and software toolkit that will enable legacy or modern CNC machines and robots to perform geometric-adaptive machining. While focused primarily on Task 2 of the Project Planning Document, the project also addresses Task 1, by creating ways to incorporate commercially-available metrology hardware into a portable toolkit solution. A summary of the proposed program is shown in Figure 1.

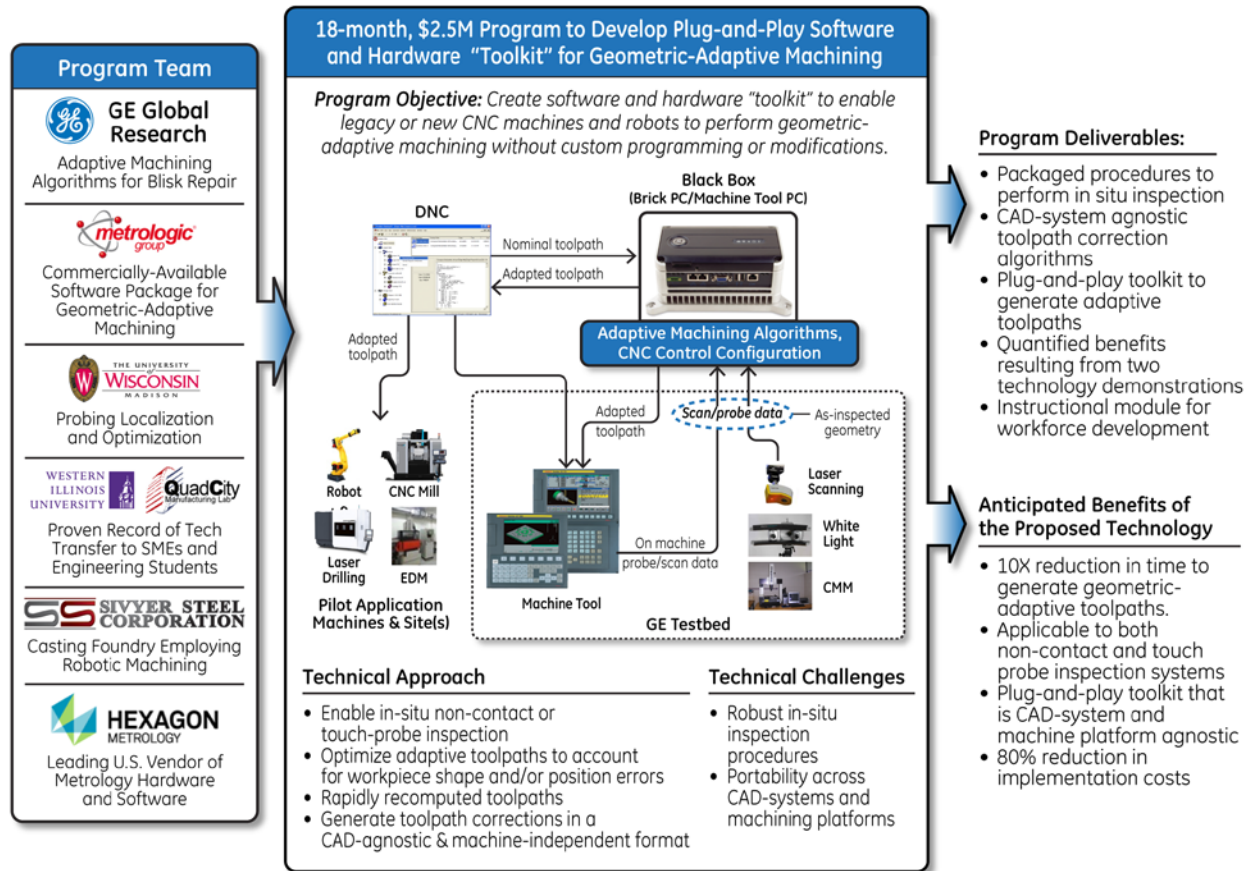


Figure 1. Summary of the proposed program.

The goal of this effort is to provide a portable, user-friendly, commercially-available tool that will reduce the development time for geometric-adaptive machining applications by 90%. In addition, implementation costs will be reduced by 80%. These benefits will be documented through a technology demonstration on adaptive casting machining, and a second demonstration that will show portability across applications, machines, and controllers. While the technology demonstration focuses on machining of castings, it leverages prior work by the team in adaptive machining of composites and turbine airfoil repair, two other applications of critical importance to the domestic commercial, and military supply chains.

II.2 PROJECT TEAM

The original project team comprise of GE Global Research (GE), Hexagon Mertology, Metrologic Group, University of Wisconsin-Madison (UWM), Sivyer Steel Corporation, and Western Illinois University Quad-City (WIU-QCML). Due to the economic downturn in the casting industry prior to the start of this project, Sivyer Steel was not able to participate in this project and needed to sell their robotic division to meet cashflow requirements. A search for a replacement company was conducted and Genesis Systems was found. Genesis Systems is a robotic integration company, and they have robot arms and end effectors that were a good match for what was proposed for Sivyer Steel's contribution to the project. The diverse team brought a variety of unique capabilities to the project.

GE Global Research has developed adaptive machining software and applications for repair and composite machining under prior internal and government programs. GE Global Research in the past has successfully demonstrated adaptive machining at TRL4 for blisk machining application that involve multiple key technologies for morphing toolpaths. In this program, GE developed the advanced geometric adaptive algorithms for implementation into the toolkit. Hexagon is the leading U.S. developer and vendor of contact and non-contact metrology hardware and software, and was a partner in GE's previous work on adaptive composites machining. The metrology system used in this program were acquired from Hexagon.

Metrologic Group is a commercial vendor of state-of-the-art adaptive machining software, range of 3D inspection software, and software/hardware integration capabilities. Metrologic has successfully demonstrated adaptive machining for an aerospace customer and interfaced their technologies with various machine tool controllers and robotic systems and is the world's leading provider of independent 3-D metrology software that is used by over 4000 companies. In this program, geometric adaptive machining algorithm is integrated as a workflow module into their existing software package. University of Wisconsin-Madison (UWM) has significant and documented expertise in probing localization and optimization. In this program, UWM developed probe point selection algorithm that automate the selection of probe points, enabling a more robust and efficient touch-probe measurement schemes.

Western Illinois University's Quad-City Manufacturing Lab (QCML) has extensive experience and a proven record of disseminating new manufacturing technologies to engineering students, local SMEs, and the Department of Defense (DoD). WIU-QCML and Genesis Systems provided the platform to deploy and test the geometric adaptive machining solution for both CNC machine tools and robots.

II.3 ADAPTIVE MACHINING BACKGROUND

Geometric adaptive machining uses metrology data to customize tool to accommodate component shape variation. A few key elements necessary to successfully implement adaptive machining solutions are:

- Accurate measurement of part geometry
- Correct registration of inspection data to nominal geometry
- Calculation of model geometry deviations to determine required tool path modifications
- Visualization tools that enable an operator to quickly adjust programs for adaptive machining

The standard process for implementation is highly manual and requires a team of manufacturing experts with skills in inspection process development, computational geometry, and advanced NC code generation for specific controllers. This level of experience is typically gained over time. Even in large

corporations, there are typically just a handful of capable experts with the requisite skills. This is also a highly iterative process that is error prone and requires the availability of experts through all stages of process development, including production. As shown in Figure 2, the current process for developing a closed-loop adaptive machining solution requires anywhere from 3 to 6 months.

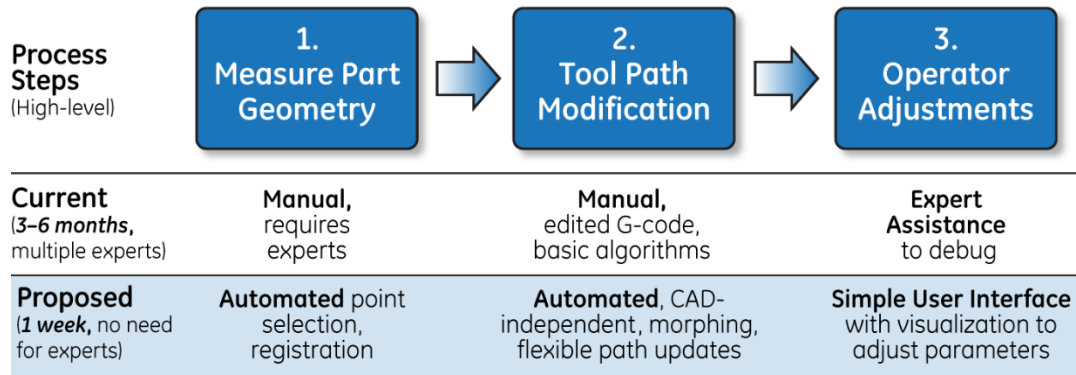


Figure 2. Adaptive machining process map comparison.

The state-of-the-art in-situ measurement technology for adaptive machining is on-machine touch probing, which is typically used for gaging and on-machine qualification. However, touch probes increase the process cycle time significantly, each probe point typically takes 20 seconds to acquire. Also, although Polyworks, Rapidform, and Metrologic currently offer tools to modify geometry based on measured data, but they typically perform simple offsets or rigid body transformations.

Relative to adaptive machining, there are currently a few available commercial solutions, with TTL providing the most commonly deployed adaptive machining package. However, custom software development is required for each new application, part geometry, and machine/controller combination. Furthermore, toolpath modifications provided by TTL are CAD/CAM system specific. Beyond these commercially available solutions, some companies have developed toolpath modification schemes that use simple linear interpolations embedded in G-code, but these interpolations are not sufficient to model the highly non-linear distortion often found in applications that require adaptive machining.

Table 1 summarizes the status of the current solutions. What is evident from this table is that although specific solutions do exist for the various technologies required to perform geometric-adaptive machining, these solutions often exist as islands, and there is no workflow tool that is capable of integrating all the data streams into a single digital thread.

Table 1. Status of the current solutions and highlights.

Technology	Currently Available Solutions
On-machine measurement	<ul style="list-style-type: none"> Utilize touch probes to collect measurement data. User must “register” measurement data to the coordinate system of the part and/or the machine tool or robot
Geometry and/or Toolpath modification	<ul style="list-style-type: none"> Simple offsets, rigid body transformations based on measured data (Polyworks, Rapidform, Metrologic) Linear interpolations embedded in G-code (proprietary) Geometry re-creation from inspection data (TTL, BCT Gmbh)
CAD/CAM System Integration	<ul style="list-style-type: none"> Tools to perform toolpath modification are CAD/CAM system specific (TTL)

Machine tool or robot controller	<ul style="list-style-type: none"> Integrated controller based on one machine (TTL)
New geometric-adaptive implementations	<ul style="list-style-type: none"> Customization of software for each new application must be done by software vendor (e.g., TTL or BCT GmbH)
Adaptive Machining Workflow	<ul style="list-style-type: none"> No single solution to integrate data flow between the CAD/CAM, data collection, and toolpath modification systems

II.4 Technical Approach

The scope of the project was to develop a geometric adaptive machining (GAM) solution that adapts nominal toolpaths to compensate for as-is geometric variation. To address the gaps highlighted in Table 1, this program focused on guiding the selection of probe points, improving the robustness of geometric adaptive algorithms, automating the selection of these algorithms, and linking each of these elements through a user interface that will enable a shop-floor manufacturing engineer to configure and execute GAM solutions. The plug-and-play solution that was developed is agnostic to machine tool or robot controller. The team also demonstrate the plug-and-play aspect of the software solution by enabling shop-floor engineers who handle conventional tool path programming to design and implement a geometric adaptive machining solution. In addition to demonstrating ease of use of the plug-and-play solutions, these demonstrations allowed the team to quantify the expected benefits of this approach.

To meet the aggressive goal of completing the project in 18 months, the team focused on integrating inspection technologies which have the highest probability of advancing the state-of-the art. For example, because current commercial off-the-shelf (COTS) non-contact metrology systems have not been sufficiently leveraged for geometric adaptive machining, the team developed techniques to correctly set-up and use these COTS devices in-situ to support geometric adaptive machining. This allowed the team to demonstrate cycle time reductions without needing to invent new interfaces for on-machine non-contact measurement systems.

III KPI'S & METRICS

Metric	Baseline	Goal	Results	Validation Method
Enter Metric	Enter Baseline	Enter Goal	Enter Results	Enter Validation Method
Time to develop adaptive machining solution	3-6 months	1 week	1 week	WIU-QCML used the toolkit to develop adaptive machining in one week for a blind used case
Investment cost to implement new geometric adaptive machining (GAM) solutions	\$1.25M	\$250K	~ \$250K	WIU-QCM demonstrated using GAM on a low-cost HASS CNC machine
Cost to retrofit existing controller with GAM	\$250K	\$50K	\$25K - \$60K	WIU-QCML used toolkit to develop and demonstrate

				GAM solution on HASS CNC and Fanuc robot
Expertise required to develop adaptive machining solution	Research and Development – advanced degrees	CAM Programmer experience	CAM Programmer	Users with basic CAM programming experience used the toolkit to develop adaptive machining solution for CNC and robots
Compatibility with machine control	Controller specific	Machine control agnostic	CNC machine tool agnostic	Live demo on HASS control and virtual demo on Fanuc and Siemens control using Vericut simulation

IV TECHNOLOGY OUTCOMES

IV.1 SYSTEM OVERVIEW

The geometric adaptive machining (GAM) toolkit intends to provide an approach that simplifies the implementation process by providing modules that are integrated into Metrologic commercial software Metrolog as workflow. The workflow approach in Metrolog enable users to define-workflow for specific inspection methods, machine tool, or robot and the type of adaptation required. This modular approach drives some key requirements this solution addresses:

- Ability to interface with different inspection methods including, but not limited to, on-machine touch probing and non-contact in-situ measurement using laser trackers or scanners
- Robust approaches to ingest and manipulate point cloud data
- CAD platform independence - the geometric algorithms are developed on Parasolid geometric kernel, which is the kernel of choice for most CAD tools
- User-selectable menu of tool path adaption schemes that enable the operator to:
 - Define methods to compute and apply rigid body transformations to modify toolpath program
 - Morph toolpath program by applying a non-linear deformation map to modify the toolpath
 - Model as-measured geometry from inspection data, mapping nominal toolpath to as-measured geometry, or regenerating the toolpath program
 - Toolpath program are modified at G-code level for CNC machine tool, thus making the system CAM independent
- Customizable operator interface

The various steps of the GAM process map, and required expertise, are shown in Figure 3

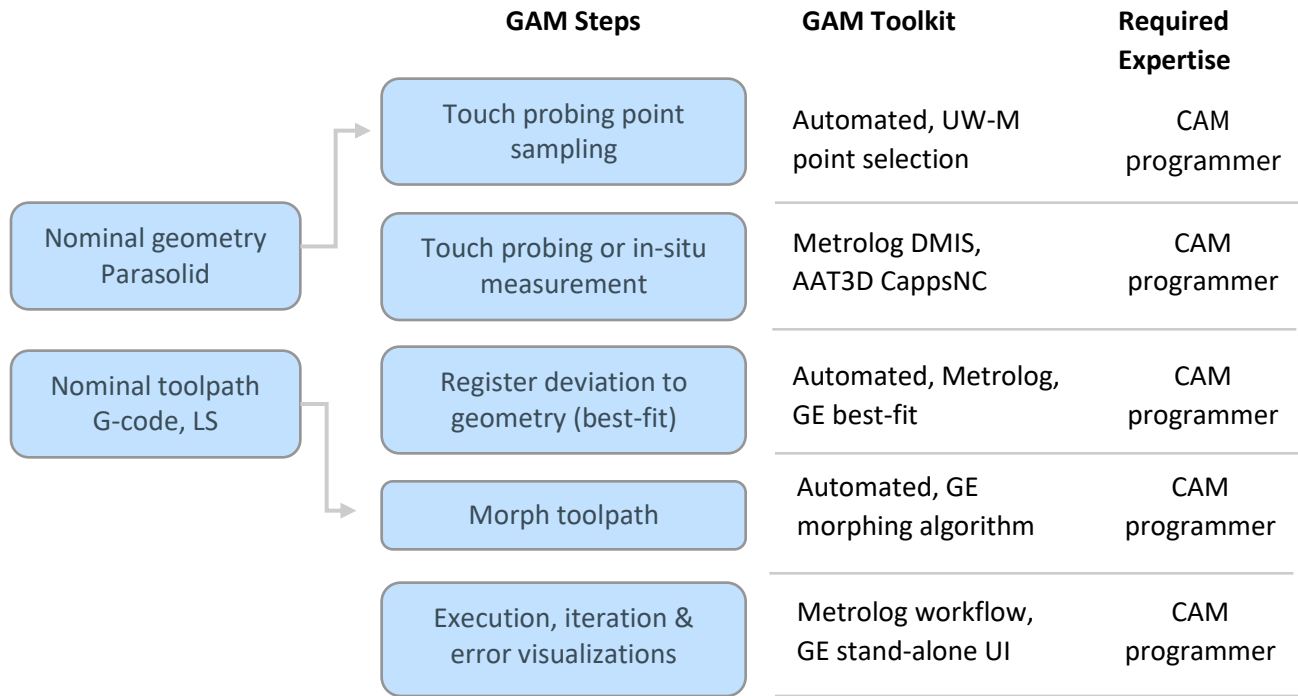


Figure 3.1. Process steps for adaptive machining

IV.2 Touch Probe Measurement

Touch probe point sampling is done using University of Wisconsin Madison point selection tool that was developed under this program. The algorithm is detailed in subsequent subsections.

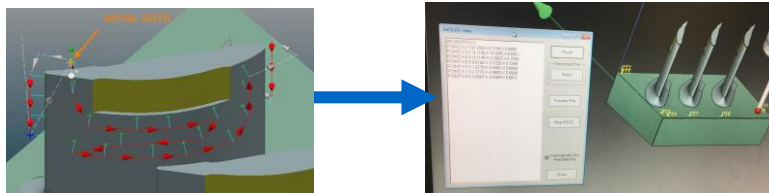


Figure 4.1. Probe path planning in Metrolog and converted from DMIS to G-code

Touch probe path planning is done using Metrolog inspection software. The probe path program is generated as a DMIS format. AAT3D CappsNC is used to convert the DMIS format into G-code that can be run on the machine tool.

IV.3 Touch Probe Point Sampling Algorithm

Point selection is a key step that occurs first in the process map for GAM. In practice, point selection is driven by the algorithm used for geometry adaptation. The final probe points chosen for a specific part shape must address geometric accessibility and minimize inspection efficiency while ensuring that the collected data allows one to accurately model the actual geometry of the component. The existing CMM sampling approach is an intuitive idea to find the point set that best resembles the

original CAD geometry. This is usually an iterative process where the sampled points are first fitted by a NURBS. The deviation between the fitted NURBS and original CAD geometry is then compared.

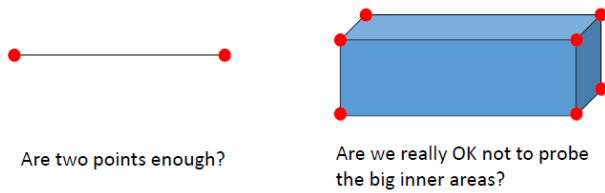


Figure 4.2. Approximate the geometries with planar surfaces.

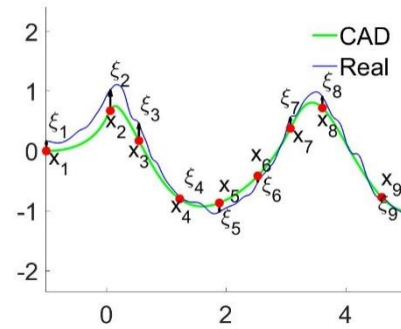


Figure 4.3. Deviation $\xi(x)$ between the real part (blue curve and the CAD model (green curve).

A point is added at the place of maximum deviation and iterate. In the literature, general methods for surface sampling include clustering-based approach, iterative simplification, direct sampling approaches, particle simulation and geometric approximation. The clustering-based approach splits the surface into several subsets, each of which is replaced by one representative sample. The iterative simplification approach successively collapses point pairs (edges, faces) in a point cloud (polygonal meshes) according to the point-to-surface distances. The direct sampling approach include the low discrepancy sampling, the stratified sampling, and uniform sampling in parametric domain. The particle simulation approach computes new sampling positions by moving particles on the surface according to inter-particle repelling forces. The geometric approximation methods trying to find the L^p -optimal piecewise-linear approximation to a smooth function by the sampling points. Such geometric approximation and optimization methods are not widely used due to the heavy computational burden. It has been proven that that L_1 - optimal polygonal approximation of convex surfaces is NP-hard.

In this work we developed a computer method for measuring surface deviations between the machined part and the nominal geometry due to machining errors. The measured surface deviations are then used to adjust the machining tool path. Here, touch probing by the coordinate measurement machine (CMM) is used to inspect the surface deviations. As such, we need to determine suitable points for the touching probing. A surface uncertainty-based approach was developed to maximize the amount of information acquired by the touch probing of the surface deviations caused by machining errors. The surface uncertainty is modeled by the Gaussian process model and the probing points are selected to minimize the maximum surface uncertainty (surface variance) conditioned on the touch probing at the selected points. The algorithm was tested with various numerical examples and was applied in real machining scenarios. The surface reconstruction error based on the developed algorithm is 50% smaller than uniform sampling. The experiments of on machine probing has validated that the selected points can adequately capture the machining errors. The algorithm and technique that was developed for choosing the optimal probe points is outlined in the following sections.

Gaussian Process in Adaptive Sampling

In geological and environmental literature, the universal kriging is used to model the spatial variation of the target variable:

$$z(\mathbf{x}) = \sum_{i=1}^m \beta_i f_i(\mathbf{x}) + \xi(\mathbf{x}), \quad (2)$$

where $z(\mathbf{x})$ is the target variable at location \mathbf{x} , $\{f_i\}$ are the co-variates, $\{\beta_i\}$ are regression coefficients, and ξ is the residual. The universal kriging model contains two parts: the overall trend, which is usually modeled by linear regression, and the residual, which is usually modeled as a stationary, spatially autocorrelated process like Gaussian Process (GP). The universal kriging variance is used to evaluate the prediction uncertainty, which incorporates both the variance of the residual and the variance of the trend. The sampling points are selected by minimizing the average of the universal kriging variance at points by simulated annealing. Similar adaptive sampling strategies that aims at minimizing the prediction error (uncertainty) have also been applied.

In touch probing, the target variable is the coordinate of the part in the probing direction $z(\mathbf{x})$ at location \mathbf{x} . Assuming $z^{\sim}(\mathbf{x})$ is the corresponding coordinate on the CAD model, we have

$$z(\mathbf{x}) = z^{\sim}(\mathbf{x}) + x(\mathbf{x}); \quad (3)$$

where z is the coordinate of the real part, z^{\sim} is the nominal coordinate on the CAD model, and x is the residual deviation between the real part and the CAD model.

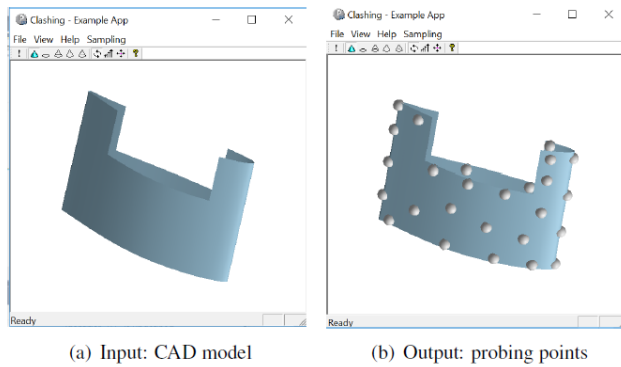


Figure 4.4. Point selection for touch probing

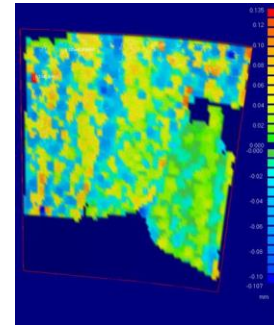


Figure 4.5. Airfoil deviation plot

Compared with the sampling design for predicting geological and environmental variables, in our application the overall trend $z^{\sim}(\mathbf{x})$ of the target variable is known with the nominal CAD model and we are only interested in the deviation $\xi(\mathbf{x})$. If the residual deviations at different locations are jointly Gaussian distributed, we predict the surface deviations at un-probed points by the measurements at probed points by Gaussian process regression (kriging) and select sampling points to minimize the maximum variance of the predictions.

Minimizing the Uncertainty of the Sampled Surface Deviations

As shown in Figure 4.4 the input of our approach is the nominal CAD model, and the output are the positions of the probing points. The optimal probing points are selected to minimize the maximum surface variance conditioned on the measurements at the probing points:

$$\min_{\mathbf{x}_1 \dots \mathbf{x}_n} \max_{\mathbf{x}} \text{var}(\xi(\mathbf{x}) | \xi(\mathbf{x}_1) \dots \xi(\mathbf{x}_n)), \quad (4)$$

where $\mathbf{x}_1 \dots \mathbf{x}_n$ are the positions of the probing points, $\xi(\mathbf{x}_1) \dots \xi(\mathbf{x}_n)$ are the measurements of the surface deviation at

the probing points, and $\text{var}(\xi(\mathbf{x}) | \xi(\mathbf{x}_1) \dots \xi(\mathbf{x}_n))$ is the surface variance conditioned on the measurements.

In this work we assume that the surface deviation measured at a single point follows Gaussian distribution, with zero mean (unless we know the specific bias) $E(\xi(\mathbf{x})) = 0$ and variance $\text{var}(\xi(\mathbf{x})) = \eta + \gamma$, where η is the variance of the machining error, it is known (or can be estimated) for a certain system, and γ is the variance of the measurement error for the CMM machine. The auto covariance between the deviations at two points is

$$\text{cov}(\xi(\mathbf{x}_i), \xi(\mathbf{x}_j)) = \eta \exp\left(-\frac{\|\mathbf{x}_i - \mathbf{x}_j\|^2}{2\sigma^2}\right) + \gamma\delta_{ij}, \quad (5)$$

where η and γ are as defined before, $\delta_{ij} = 1$ when $i = j$, and $\delta_{ij} = 0$ when $i \neq j$, σ is the characteristic length of the surface deviations, it can be estimated from the past samples of machined parts. When the surface deviation is smooth we have large σ , and when the surface deviation oscillates we have small σ . Figure 4.5 shows surface deviations of the machined airfoil to the nominal CAD geometry. In this case the deviation has moderate oscillations, if the overall width of the airfoil is L , the characteristic length σ of the surface deviation $\xi(\mathbf{x})$ could be set around at $L/6$.

Based on the statistical characteristics of $\xi(\mathbf{x})$, we have the joint distribution of the surface deviations at points $\mathbf{x}_1 \dots \mathbf{x}_{n+1}$ follow the multivariate Gaussian distribution:

$$p(\xi_1, \xi_2, \dots, \xi_{n+1}) \sim N(\mathbf{0}, \Sigma), \quad (6)$$

where $N(\cdot; \cdot)$ means the Gaussian distribution, with the first parameter its mean and the second parameter its covariance matrix, Σ is the $(n+1) \times (n+1)$ covariance matrix, which can be partitioned by:

$$\Sigma = \begin{bmatrix} \mathbf{C}_{n \times n} & \mathbf{V}_{n \times 1} \\ \mathbf{V}_{1 \times n}^T & c \end{bmatrix}, \quad (7)$$

where $C_{ij} = \text{cov}(\xi(\mathbf{x}_i), \xi(\mathbf{x}_j))$, $V(i) = \text{cov}(\xi(\mathbf{x}_i), \xi(\mathbf{x}_{n+1}))$, and $c = \text{cov}(\xi(\mathbf{x}_{n+1}), \xi(\mathbf{x}_{n+1}))$. Given the observations of the surface deviations $\xi_1 \dots \xi_n$ at the points $\mathbf{x}_1 \dots \mathbf{x}_n$, the conditional distribution of the deviation at \mathbf{x}_{n+1} is:

$$p(\xi_{n+1} | \xi_1 \dots \xi_n) \sim N(\mathbf{V}^T \mathbf{C}^{-1} \boldsymbol{\xi}, c - \mathbf{V}^T \mathbf{C}^{-1} \mathbf{V}), \quad (8)$$

where $\mathbf{V}^T \mathbf{C}^{-1} \boldsymbol{\xi}$ is the conditioned mean, which is the maximum likelihood estimation of \mathbf{x}_{n+1} based on the previous n observations, and

$$\text{var}(\xi(\mathbf{x}_{n+1}) | \xi(\mathbf{x}_1) \dots \xi(\mathbf{x}_n)) = c - \mathbf{V}^T \mathbf{C}^{-1} \mathbf{V}, \quad (9)$$

is the conditional variance of \mathbf{x}_{n+1} , which tells how much variations \mathbf{x}_{n+1} can have given the observations of $\xi_1 \dots \xi_n$

In the following section a next-best-point algorithm is developed for the probing points selection by equation (4).

Next-Best-Point Algorithm

Given a CAD model (represented by trimmed NURBS surfaces), it is discretized into a point cloud by densely sampling in the parametric domain (the surface in Figure 4.6 contains 1200 points), then n number of probing points are selected from the point cloud based on equations (4) and (9), which minimizes the maximum conditional uncertainty of the surface deviations. The number of points N contained in the point cloud is usually several orders of magnitude larger than the number of probing points n . Directly selecting n number of points from the dense point cloud (contains N number of points) of the nominal CAD model by equation (4) needs $C_N^n = N!/n!(N-n)!$ number of function evaluations

of (9), which is computationally prohibitive, especially when N is large. Here, a heuristic algorithm that adds probing points one by one is developed:

Stage I: next best point selection:

1. Start from one point selected at the corner or at the place of maximum curvature, we have the sampled set
 $S = [x_{j1}]$.
2. Calculate the conditional variances $\text{var}(\xi(x)|S)$ at different points x on the CAD model, if $\max_x \text{var}(\xi(x)|S) < \varepsilon$, stop, else, go to step 3.
3. Add the point that maximizes (9) into the set S , go to step 2

Stage II: simultaneously adjust the sampled set $S = \{x_{j1} \dots x_{jn}\}$ to reduce the effects of different initial points:

1. Fix $n-1$ points in S , find the best position for the remaining one that maximizes (9).
2. Fix another $n-1$ points and adjust the remaining one as in the previous step; keep iterating, until converge.

The stopping criterion in stage I is set at $\varepsilon = 4\gamma$:

$$\max_x \text{var}(\xi(\mathbf{x})|\xi(\mathbf{x}_1) \dots \xi(\mathbf{x}_n)) \leq 4\gamma, \quad (10)$$

where γ is the square of the precision of the coordinate measurement machine. Since it is impossible to push the sampling precise beyond the measuring precision, it may be wise and economic to stop at the place of two standard deviations $2 \cdot \text{sqr}(\gamma)$. In some cases, the users may decide the number of probing points by themselves and in such situations the algorithm can tell the users the sampling precision at the end by equation (9). However, since stage I is essentially a greedy search, its result is affected by the selection of the first point. By equation (5), initially all points have the same variance, so the first point is selected by other criteria like maximum curvature point or corner point, which are non-optimal with regard to minimizing the surface uncertainty. In order to eliminate the effect of first point selection, stage II of simultaneously adjustment is added. Figure 4.6 shows the process of

probing point selection on a 3D surface by our algorithm. The color shows the value of the conditional surface variance (9).

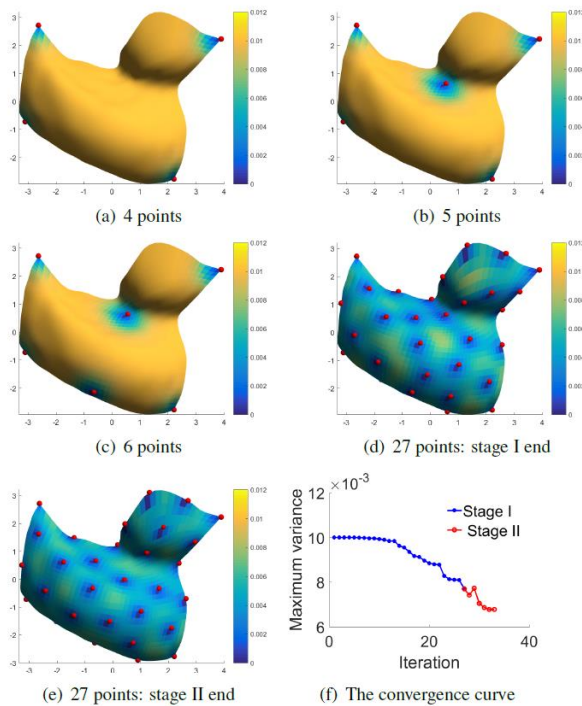
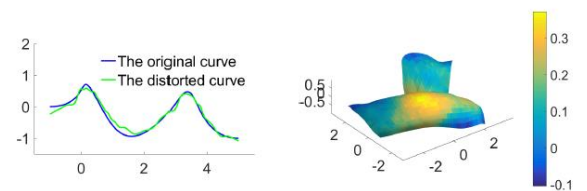


Figure 4.6. The next best point algorithm, color shows the value of conditional surface variance.

It could be seen that in stage I the maximum variance monotonically decreases as the number of sampling point increases, while in stage II the maximum variance is not monotonically decreasing. That's because in stage I with the sampled set S fixed, the added point will further reduce the surface uncertainty, while in stage II each time the sampled set S is slightly different.

Evaluation Metric



(a) Simulated deviations on a curve (b) Simulated deviations on a surface

Figure 4.7. Simulating the surface deviations caused by machining.

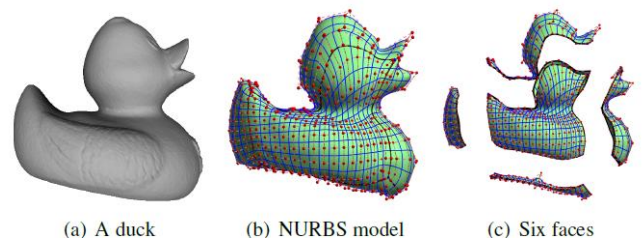


Figure 4.8. A duck model composed by six NURBS surfaces.

In order to validate the developed approach, deviations on the surface caused by machining errors are randomly simulated by the Gaussian process with mean $E(\xi(\mathbf{x})) = 0$ and auto covariance $\text{Cov}(\xi(\mathbf{x}_i), \xi(\mathbf{x}_j)) = 0.03 \exp(-\|\mathbf{x}_i - \mathbf{x}_j\|^2/2) + 0.003 \exp(-\|\mathbf{x}_i - \mathbf{x}_j\|^2/2 * 0.1^2) + 0.0003 \delta_{ij}$. Here the auto covariance is designed to be different than the auto covariance in equation (5) by adding the term $0.003 \exp(-\|\mathbf{x}_i - \mathbf{x}_j\|^2/2 * 0.1^2)$, which represents small scale high frequency oscillations in the surface deviations (with smaller variance and shorter characteristic length). Since in practice the true auto covariance of the deviation can't be known, and we can only have estimations based on past observations, so it is more objective to make the two auto covariances different in experiments (one is used to generate the deviations and one is used in the sampling algorithm). Figure 4.9 shows simulated deviations on a 2D curve and on a 3D surface. In this research $m = 100$ sets of surface deviations are randomly simulated for each CAD model. Note that the simulated deviations are $\hat{\xi}(\mathbf{x})^{(i)}, i = 1, \dots, m$. Given the probing points $\mathbf{x}_{j1}, \dots, \mathbf{x}_{jn}$ defined on the CAD model, we can measure corresponding deviations $\xi(\mathbf{x}_{j1})^{(i)}, \dots, \xi(\mathbf{x}_{jn})^{(i)}$, based on which a smooth reconstruction of the surface deviations can be obtained $\tilde{\xi}(\mathbf{x})^{(i)}$ by the Gaussian process regression, the reconstruction errors

$$\begin{aligned}
 E^{(i)} &= \int_{\Gamma} \|\tilde{\xi}(\mathbf{x})^{(i)} - \hat{\xi}(\mathbf{x})^{(i)}\|^2 d\mathbf{x} \\
 &\approx \sum_{j=1}^N \|\tilde{\xi}(\mathbf{x}_j)^{(i)} - \hat{\xi}(\mathbf{x}_j)^{(i)}\|^2
 \end{aligned} \tag{11}$$

are used to evaluate the effectiveness of the selected probing points. Here N is the total number of points in the point cloud that represents the CAD model.

Method of Validation

The probing points selected by the proposed approach (note as Gaussian process model (GPR) based approach) are compared with the probing point selected by the uniform sampling in parametric domain (note as uniform sampling), the heuristic algorithm that aims at minimizing the approximation error of the nominal CAD model (1) (Note as NURBS deviation based approach), and the NURBS uncertainty based algorithm that aims at minimizing the uncertainty of the approximation of the nominal CAD model (note as NURBS uncertainty based approach). The six surfaces of the duck model as shown in Figure 4.8 are used for the testing.

Figure 4.9 shows the probing points sampled on the front face of the duck model by the proposed approach, the NURBS uncertainty-based approach, the NURBS deviation-based approach, and the uniform sampling.

Figure 4.9. Probing points sampled on the front face of the duck model by (a) the proposed approach, (b) NURBS uncertainty-based approach, (c) NURBS deviation based heuristic algorithm, (d) uniform sampling.

Figure 4.11. Probing points sampled on the front face of the duck model by (a) the proposed approach, (b) NURBS uncertainty-based approach, (c) NURBS deviation based heuristic algorithm, (d) uniform sampling.

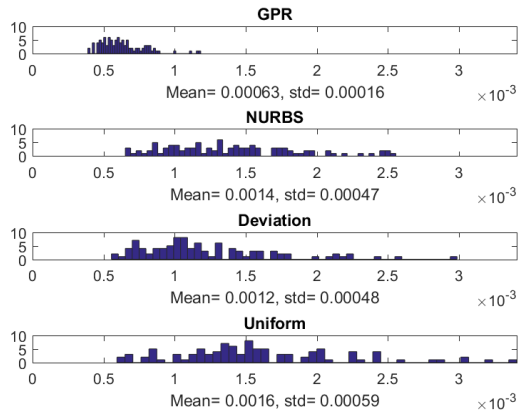


Figure 4.10. Histogram of the reconstruction errors of the four approaches for the 100 sets of deviations randomly generated on the front face of the duck model. The vertical axis shows the number and the horizontal axis shows the reconstruction error in the units of square meter.

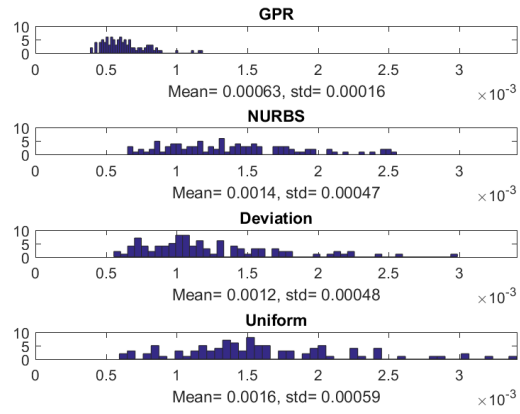


Figure 4.12. Histogram of the reconstruction errors of the four approaches of 100 sets of deviations randomly generated on the bottom face of the duck model. The vertical axis shows the number and the horizontal axis shows the reconstruction error in the units of square meter.

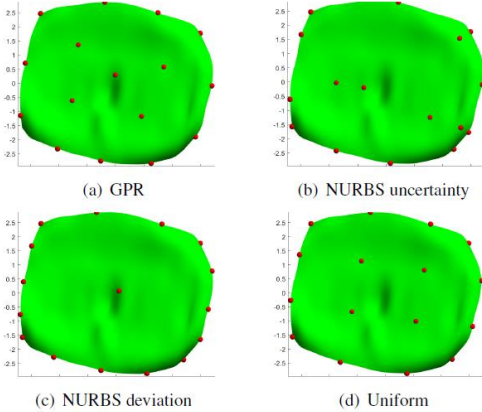
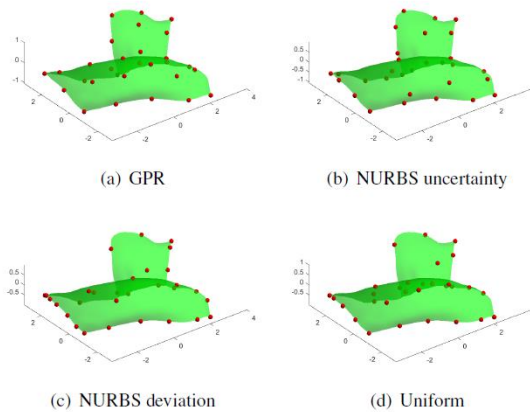


Figure 4.10 shows the histogram of the reconstruction errors based on the probing points selected by the four approaches for the 100 sets of randomly generated surface deviations on the front face of the duck model. It can be seen the proposed approach gives the smallest reconstruction errors while the uniform sampling approach gives the biggest reconstruction errors. Figure 4.11 shows the probing points sampled on the bottom face of the duck model by the proposed approach, the NURBS uncertainty-based approach, the NURBS deviation-based approach, and the uniform sampling. Figure 12 shows the histogram of the reconstruction errors based on the probing points selected by the four approaches for the 100 sets of randomly generated surface deviations on the bottom face of the duck model.

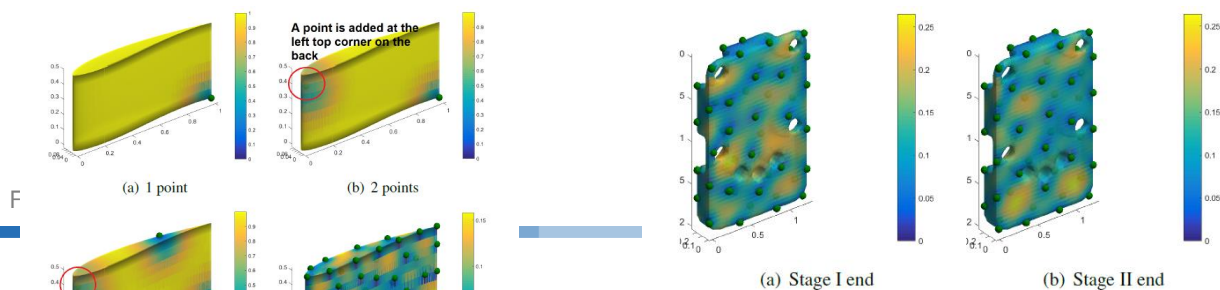


Figure 4.13. Probing point selection for the airfoil model, color shows the value of the conditional surface variance.

Figure 4.14. Probing point selection for the sensor adapter, color shows the value of the conditional surface variance.

It can be seen the proposed approach gives the smallest reconstruction errors while the NURBS uncertainty-based approach and NURBS deviation-based approach give the biggest reconstruction errors. That's because the foregoing two approaches aim at approximating the nominal NURBS surface, so very few probing points are put in the middle flat area, since the bottom face of the duck model is almost flat except on the boundary and in the center. However, the simulated surface deviations oscillate on the bottom face, whose pattern is similar as in Figure 4.5 and 4.7. The testing results on all the six surfaces of the duck model suggest that the proposed approach is superior over the other three approaches.

Numerical Examples

In this section, we show the results of probing points selection on various CAD models. Figure 4.13 shows the process of probing point selection for the airfoil model. Starting at a point in the right lower corner, the second point is chosen to be a point on the left top corner and we can see the maximum surface uncertainty, the third point is added at the top edge, the fourth point is added at the bottom edge, and the fifth point is added at the left lower corner. By the end of stage I we have selected 50 points. The algorithm tries to distribute the points as evenly as possible on the CAD model. After the simultaneous adjustment in stage II, the probing points distribute evenly on the CAD model and successfully capture the features like corners, edges, and high curvature areas. The maximum surface uncertainty decreases fast in the stage of next best point search and converges in a few iterations in the stage of simultaneous adjustment.

Figure 4.14, 4.15, and 4.16 shows the two stage sampling results of the sensor adapter, plug handle, and the spinner. The developed algorithm handles those complex geometries well, the sampled points distribute evenly on the models and successfully captures the edges and corners. In all the cases, the sampling results of stage II have been improved upon the results of stage I. For

example, in Figure 4.14, the sampling results of stage I failed to capture some of the corners like the corners on the top and on the left side, while the results of stage II successfully captured these points. The maximum surface variances at the end of stage II are slightly smaller than that of stage I in all the cases, which means the distribution is evenner.

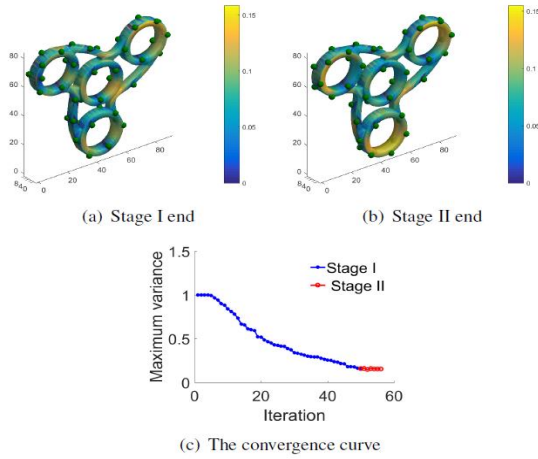


Figure 4.15. Probing point selection for the plug handle, color shows the value of the conditional surface variance.

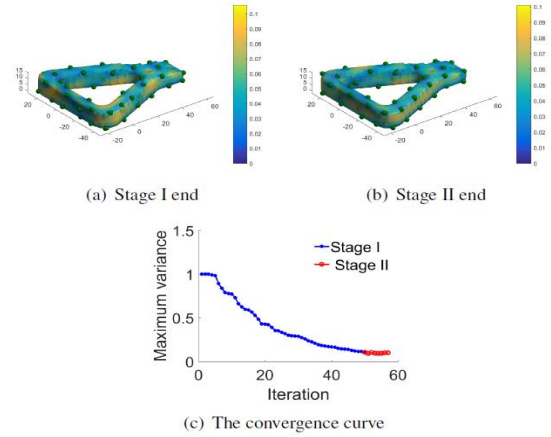


Figure 4.16. Probing point selection for the spinner model, color shows the value of the conditional surface variance.

Algorithm Improvement

In our Gaussian process model, the auto-covariance of the surface deviations at two different points is calculate by the Euclidean distance between the two points as in equation (5). However, when the model has thin structures, the Euclidean distance-based auto-covariance will cause some problems. As shown in Figure 19, by the Euclidean distance d_1 , \mathbf{p}_1 and \mathbf{p}_2 are highly correlated. However, in the manufacturing, \mathbf{p}_1 and \mathbf{p}_2 will have little correlation according to the machining path. So, it is more reasonable to calculate their covariance by the geodesic distance d_2 , as shown by the red curve in Figure

16. Now we have the auto-covariance calculated by geodesic distance:

$$\text{cov}(\xi(\mathbf{x}_i), \xi(\mathbf{x}_j)) = \eta \exp\left(-\frac{d^g(\mathbf{x}_i, \mathbf{x}_j)^2}{2\sigma^2}\right) + \gamma\delta_{ij}, \quad (12)$$

on the 3D surface. The meaning of other parameters are the same with equation (5). Figure 18 shows different sampling results obtained by calculating the auto-covariance based on the Euclidean distance and the geodesic distance. In Figure 19(a) on the front face of the model, there's no sampled points in the big area within the red rectangle. That's because the points on the back face of the model has affected the sampling in the front as shown in Figure 19(b). From Figure 19(c) and Figure

19(d) the geodesic distance-based approach gives more even distributions of the sampled points. Thus, in this project, two options are provided for the sampling algorithm, the first one compute point-to-point covariance by the Euclidean distance, the second one compute point-to-point covariance by the geodesic distance, which is designed for thin structures.

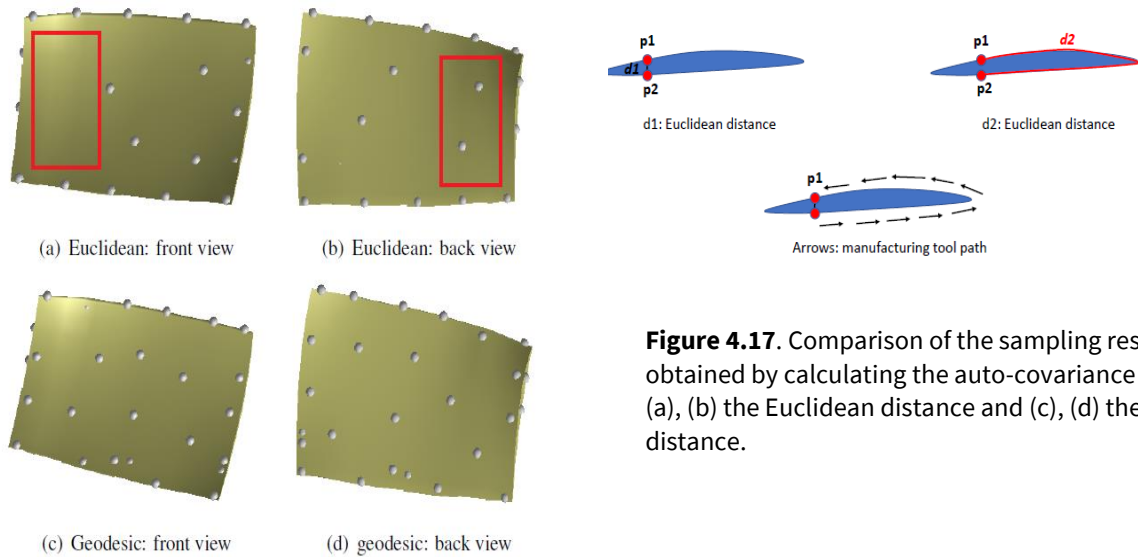


Figure 4.17. Comparison of the sampling results obtained by calculating the auto-covariance based on (a), (b) the Euclidean distance and (c), (d) the geodesic distance.

Figure 4.18. Correlation by the Euclidean distance and by the geodesic distance.

IV.4 Non-Rigid Morphing (Multi-level B-Spline) Algorithm

Multilevel B-splines interpolation and approximation (MBIA) algorithm was first introduced in 1997 by Lee et al^{31,38,39}. It has been demonstrated that it can circumvent the trade-off between the *accuracy* and *smoothness* requirements in object modeling, which is one of the most important reasons underlying the choice of this algorithm.

The *accuracy* and *smoothness* trade-off can be described as follows: with fewer B-spline control points, the reconstructed B-spline surface model from scattered points is smoother but less accurate. More control points in the B-spline surface lead to more accurate but less smooth surface. Using a well cited point cloud in Piegl's NURBS book^{Error! Reference source not found.}, this trade-off is illustrated by creating surfaces with different numbers of control points. As shown in , the B-spline surface of 32×32 patches are more accurate but less smooth than the surface of 4×4 patches, with both surfaces approximating the same point cloud.

Another reason is that it is fast and has linear time complexity w.r.t the number of data points. Let n be the number of input data points, h be the total level and d be the dimension of the tensor-product B-splines. Consider that for each level, each data point, 4^d control point values are computed. So it can be

concluded that the time complexity of the MBIA algorithm is $O(4^d hn)$. That is to say this algorithm is a linear algorithm in terms of input point number n .

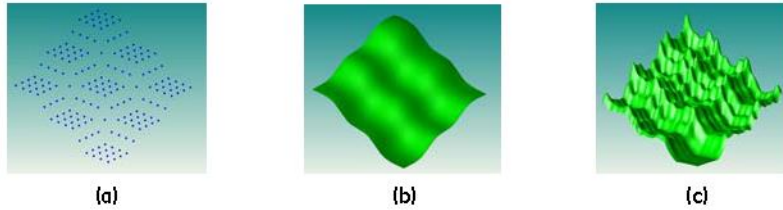


Figure 4.1.3.1. Probing Illustration of smoothness and accuracy trade-off. (a) Input point cloud from Piegls book. (b) Smooth but not accurate surface with 4x4 patches. (c) Accurate but not smooth surface with 32x32 patches.

The MBIA algorithm can be outlined as follows: 1) Fit the input data with a B-spline function with the coarsest control net (the first level), 2) Calculate the residual point set. The second level will not fit the original point set, but the new residual. The same process repeats for the following levels by fitting the residuals and generate a sequence of B-spline functions, and 3) Get the final approximated function by combining this sequence of B-spline functions using the B-spline refinement or subdivision rule. Using the data shown in 21(a) as an example, this procedure is illustrated intuitively in Figure 22.

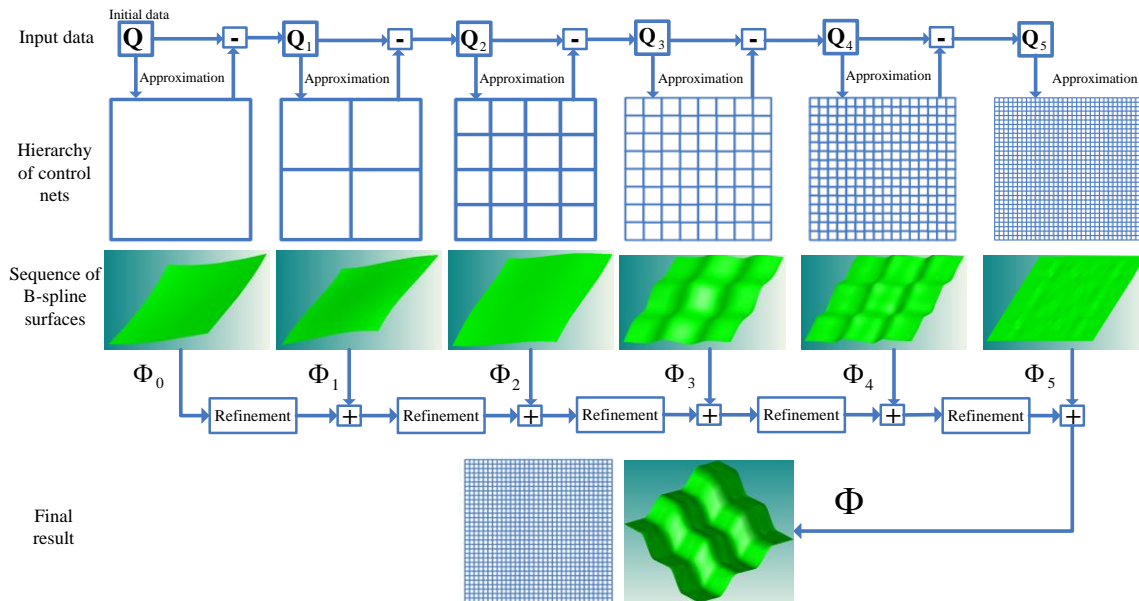


Figure 4.1.3.4. Illustration of the MBIA algorithm.

IV.5 SYSTEM REQUIREMENTS

Hardware

The geometric adaptive machining software solution is designed to run on a Windows-based PC. The computer with the necessary communication ports (RS-232 and/or Ethernet for machine communication) can be delivered preloaded with all the necessary software in the toolkit it setup and execute adaptive machining on the shop floor.

Software

As shown in figure 3.1, to execute the steps for geometric adaptive machining, the toolkit consists of software tools developed under this program and off-the-shelves commercially available software tools.

- **WIU-M Probe Point Selection:** Software tool developed under this program to automate and optimized allocation of probe points for on-machine probing.
- **Metrolog Inspection:** Commercially available inspection software, which provides an workflow oriented way of developing geometric adaptive machining solutions for CNC machine and robots.
- **AAT3D CappsNC:** CappsNC is used to convert DMIS program into g-code for on-machine probing. CappsNC is commercially available and has direct interfaces to most common CNC controllers to do real time measurement.
- **GE Morphing:** Software to perform 3D morphing of toolpath program

CAD Independence

GE's morphing algorithms were dependent on and integrated with Siemens PLM NX API. However, they are geometric algorithms that can be run using any geometric kernel. A key deliverable for this program is to develop a software solution that will enable a CAD agnostic system. In the early part of the program, various geometric kernels including ASIS, Parasolid, and Metrolog kernel were evaluated to down-select to a stand-alone implementation kernel for adaptive machining.

Parasolid geometric kernel was down-select as the kernel of choice. Parasolid is compatible to most CAD/CAM engines. The morphing algorithms were ported to Parasolid geometric kernel and demonstrated on a sample dataset. To ensure correctness, the results were compared to NX-based solution. The implementation of the morphing algorithm on Parasolid geometric kernel enable a complete stand-alone system that can be run independently

IV.6 SYSTEM ARCHITECTURE

Geometric Adaptive Machining for CNC

As shown in Figure 4.3.1, the system is design into planning and execution phase. The planning phase include generating the nominal the nominal model using any CAD/CAM system. To enable a CAD neutral platform the model is save as Parasolid model. The probe point selection tool is used to allocate the probe points on the Parasolid model. The probe path planning is done is Metrolog software which,

output a standard DMIS program. That final piece of the planning phase is to develop nominal toolpath program in the CAM environment which, is then post process in g-code format.

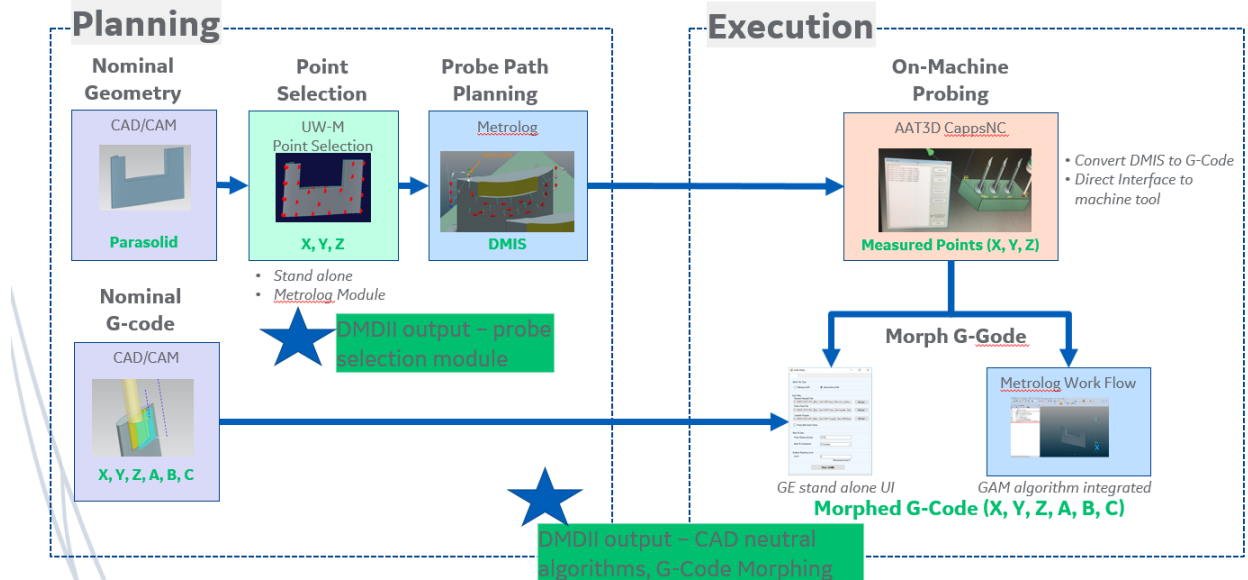


Figure 4.3.1. Geometric adaptive machining process flow for CNC machining.

In the execution phase, AAT3D CappsNC program is used to convert DMIS program into g-code for on-machine probing. CappsNC produces a generic text report with the probe points information. GE morphing algorithm uses the probe data to morph the nominal g-code program. Morphing at the g-code level enable geometric adaptive machining for CNC to be truly controller agnostic.

Geometric Adaptive Machining for Robots

The main object is to develop a plug-and-play robot system for Geometric Adaptive Machining (GAM), which will leverage the same multilevel B-spline morphing algorithm that is used for CNC adaptive machining. This system will allow a fast adjust of robot toolpath to accommodate variations in workpiece geometry and/or position. The hardware and software used to prove out robotic adaptive machining are:

- Hardware:
 - Cobalt Faro scanner
 - Genesis Fanuc robots (ARC Mate 120iC, M20-iA, etc.)
 - Plasma torch & oxy-acetylene torch
- Software:
 - Metrolog
 - Fanuc Roboguide
 - GE robot toolpath morphing toolkit

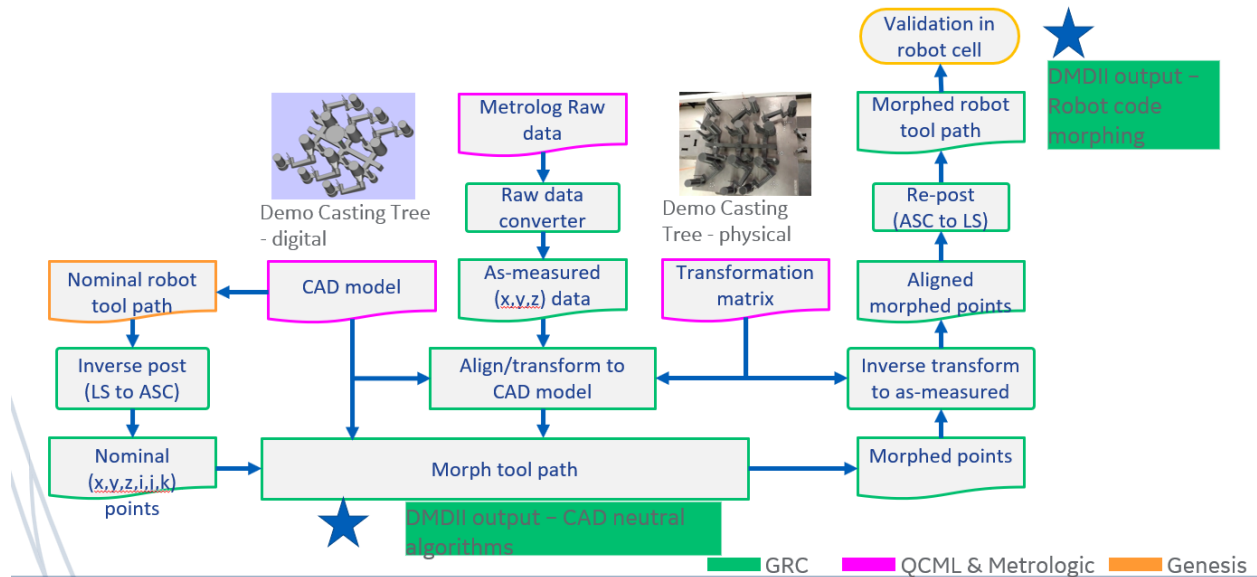


Figure 4.3.2. Geometric adaptive machining process flow for Robots

Figure 4.3.2 shows the process flow for robotic adaptive machining. Metrolog is used to align point cloud data to CAD model. GE morphing algorithm is used to modify the nominal robot path program that can be run directly on the robot.

IV.7 FEATURES & ATTRIBUTES

Specification of Touch Probe Points

Point selection is a key step that occurs first in the process map as shown in Figure 3.1. Point selection is a key step that occurs first in the process map for GAM. In practice, point selection is driven by the algorithm used for geometry adaptation. The final probe points chosen for a specific part shape must address geometric accessibility and minimize inspection efficiency while ensuring that the collected data allows one to accurately model the actual geometry of the component. In this program UWM developed a technique for choosing the optimal probe points and addresses the challenges of accessibility and inspection efficiency.

Geometry Adaptation Methods

The core algorithms that enable adaptive machining apply rigid body transformation or non-rigid morphing functions that map the nominal geometry to the as-measured shape of the workpiece. The variation in the part is captured and is used to modify the g-code.

- **Rigid Body Transformation (Best-Fit)**

In this program the algorithm for best-fit is an implementation of the Horn's algorithm [32] enhanced by selection of corresponding points using nominal surface geometry definition when available. There are two key steps in implementation of best fit:

1. Selection of corresponding points.
2. Computation of a rigid body transform that reduces the residual mean sum errors between corresponding points.

In this implementation, the measured points for the chosen nominal points are used to find the corresponding points on the nominal surface. This is obtained by computing the minimal distance to the nominal surface along the probing direction (which is typically along the normal for the nominal probe point). This solution is applicable for most case when the deviations are small compared to the thickness of the associated geometry. The flexibility of the Horn's algorithm also enables the user to lock various degrees of freedom based on the physical understanding of the problem and the chosen geometry.

- **Toolpath Morphing Strategy**

The final manifestation of geometric adaptive machining combines in-situ inspection data and algorithms for best-fitting and morphing to modify toolpath geometry. Figure 4.4.1 shows how the toolpath is morph by applying compensation to modify the nominal g-code directly.

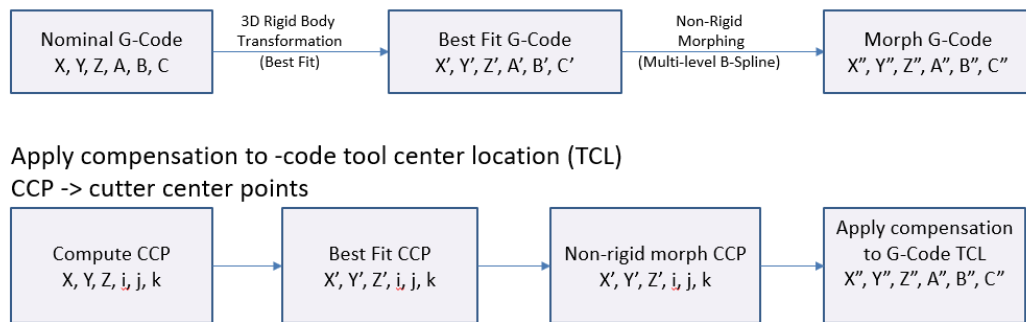


Figure 4.4.1. Morphing G-Code Algorithm

We developed Parasolid based morphing module to implement the morphing strategy with the following steps:

- Parsing g-code file to get the tool center point (TCP) and rotary angles.
- Compute the tool cutter contact point (CCP)
- Apply bestfit alignment
- Apply non-rigid morph
- Apply compensation to TCP and rotary angles

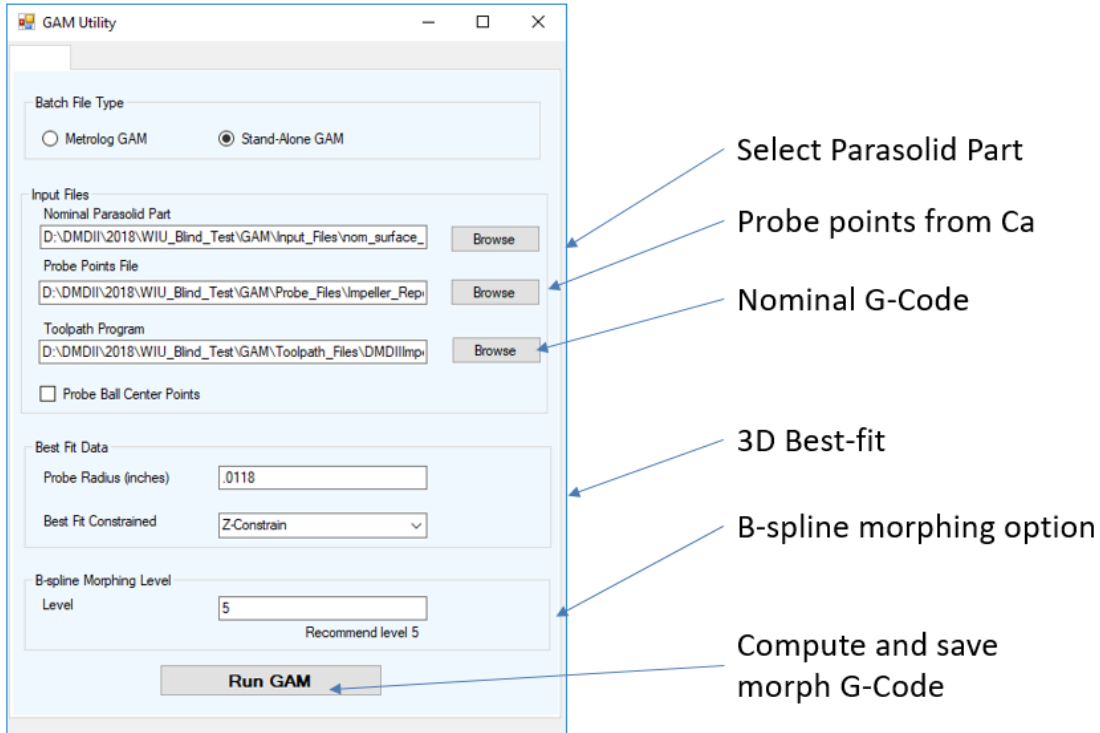
IV.8 MODES OF OPERATION

Plug-and-Play

The idea of a plug-and-play geometric adaptive solution is to enable CNC machine and robots to be retrofitted with the capabilities to perform adaptive machining. A challenge is to develop a plug-and-play solution which satisfies the many different adaptive machining scenarios that exist today. To solve this problem the geometric solution was develop as modules that can be uses to develop adaptive machining solutions and executed as one of the following options.

GE Stand-Alone Execution

Figure 4.5.1 shows the user interface that was developed to execute the GAM application as stand alone. This option uses the 3D-bestfit horns approach that is described above. How to run the stand alone version is describe in the user guide.



GAM Metrolog Workflow Execution

Figure 4.5.1. GE Stand-Alone user interface

The geometric adaptive machining toolkit modules were wrapped using macros and integrated into Metrolog commercial inspection software. As shown in Figure 4.5.2, this provides a workflow-oriented way of developing geometric adaptive machining solutions. The Metrolog interface can be used with test data for development and fine-tuning of the application. The nominal part geometry in Parasolid format will be provide to the various adaptive machining algorithms that are call via Metrolog interface as executable from the global workflow. The detail description of setting up the workflow can be found in the user guide documentation.



Figure 4.5.2. Metrolog Workflow integration with GAM g-code morphing algorithms

IV.9 USERS & USE CASES

Demonstrations of the Robotic GAM were carried out on two use cases: an adaptor arm casting and a sheet metal casting tree. The adaptor arm casting was provided by the Rock Island Arsenal (RIA) and is a component that the RIA currently manufactures. The sheet metal casting tree was fabricated from sheet metal to facilitate cutting with a plasma torch. Additionally, the sheet metal casting tree consisted of six nearly identical components that were designed to be similar to the adaptor arm casting. The Robotic GAM work utilized a Fanuc 120iC robot at Genesis Systems Group with the capability of quick-change of the end effector. A Cobalt Faro scanner was mounted on the robot for acquisition of point cloud data from the part. The data was acquired and analyzed using Metrolog software, and once the data was analyzed, it was then input to the GE morphing algorithm. The morphing algorithm calculated the deviations of the data from the nominal part, and then used the deviation values to morph the cutting paths. The adaptor arm was cut with an oxy-acetylene torch and the sheet metal casting tree was cut with a plasma torch. The morphed cutting paths in both cases were accurately located relative to the parts. The Robotic GAM reduced the time to cut the adaptor arm by more than 50% of production data provided by the RIA.

Demonstrations of the Milling GAM were carried out on three use cases: a GE airfoil, an impeller, and a swivel link. The impeller was designed as a 3D printed use case where the support material could be removed using the Milling GAM. The swivel link was designed to resemble the adaptor arm casting. The RIA requested that the Milling GAM be able to center milled features on existing cast surfaces, independent of any distortion that may exist on the part. For Milling GAM, a Haas TM-3 3-axis mill was used at Western Illinois University (WIU). A Renishaw touch probe was

incorporated into the Haas mill which was used to probe part surfaces. The probe data was collected using CAPSNC software, analyzed with Metrolog software, and then input to the GE morphing algorithm. The morphing algorithm calculated the deviations of the data from the nominal part, and then used the deviation values to morph the tool paths. The GE airfoil was produced intentionally out of spec and the Milling GAM was able to mill the probed surfaces back into compliance with the tolerance. The impeller was produced via powder bed fusion and the Milling GAM successfully removed the support material. Three out-of-tolerance swivel link prototypes were milled from aluminum blocks. The Milling GAM was able center the milled features to the existing casting within 0.20 mm (0.008”) or less. The accuracy achieved satisfies the requirements of the RIA, ensuring full strength parts.

Robotic GAM Demo

Due to the economic downturn in the casting industry prior to the start of this project, Sivyer Steel was not able to participate in this project. A search for a replacement company was conducted and Genesis Systems was found. The original files for the train engine component casting use case, which was part of the original proposal could not be used in this program. Subsequently, GE informed QCML that the Sivyer use case will not be available for use on this project. QCML approached the Rock Island Arsenal (RIA) -JMTC for casting trees, and they indicated that they should be able to provide some for use on the project.

Redesign of Casting Trees Provided by Rock Island Arsenal

The Rock Island Arsenal provided two adaptor arm casting trees from the foundry. The adaptor arm was redesigned and renamed the swivel link, so as to be safe for review by foreign nationals. In similar fashion, the adaptor arm casting tree was redesigned as the swivel link casting tree, shown in Figure 4.9.1

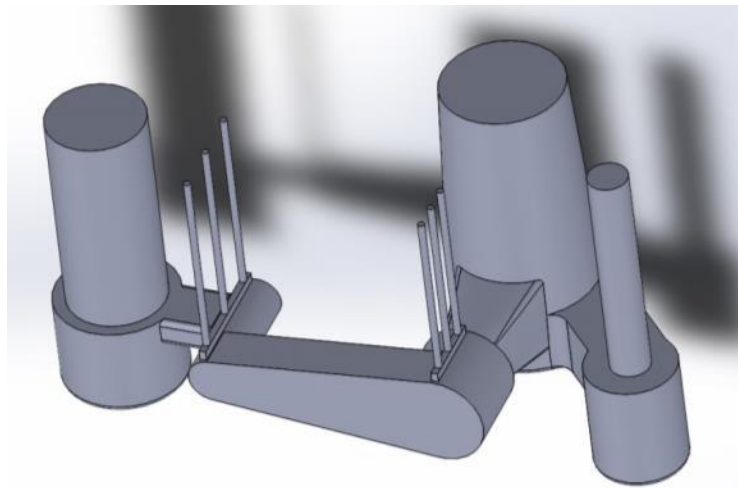


Figure 4.9.1. Solid model of casting tree for swivel link component

The SolidWorks model was used to create .stl files for the swivel link casting tree, and the .stl file was used to 3D print a scaled down plastic casting tree, shown in Figure 4.9.1. Following the successful 3D printing of the swivel link casting tree, two different cases of distortion were modeled in SolidWorks. Once again, the two different distorted solid models were used to create corresponding .stl files, and the .stl files were used to 3D print scaled down and distorted plastic swivel ink casting trees, which are shown in Figure 4.9.2 and Figure 3.9.4.



Figure 4.9.1. (left) Nominal scaled 3D polymer printed swivel link casting tree
Figure 4.9.2. (right) Distorted and scaled 3D polymer printed swivel link casting tree case #1



Figure 3.9.4. Distorted and scaled 3D polymer printed swivel link casting tree case #2

The casting trees were coated with talcum powder and then scanned into Metrolog with the romer arm integrated RSx laser scanner. An image of this process is shown in Figure 4.9.4. Two point cloud sets were captured for each part in order to capture all surfaces of the part. Any unwanted data points were filtered from the point cloud data in Metrolog, and the point cloud data sets were merged into one. The resulting assembled point cloud data sets were very large (on the order of 100M points). Consequently, the point cloud data sets underwent further Metrolog filtering (uniform filter) to remove approximately 85% of the points, resulting in point cloud sizes of approximately 10-15M points. The point cloud data is shown in Figure 4.9.6.



Figure 4.9.4. Scanning a distorted swivel link casting tree with the Romer arm scanner

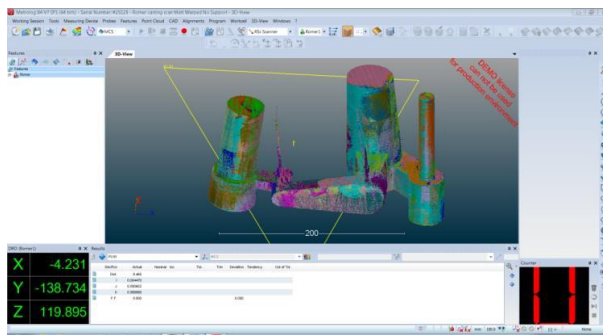


Figure 4.9.5. Point cloud produced from scan of swivel link casting tree

Several different operations were performed on the filtered & assembled point cloud data sets. First, the nominal CAD model of the swivel link casting tree was imported into Metrolog as a Parasolid file and then fit to the point cloud data set. The solid model and point cloud are shown in Figure 4.9.6. Once the fitting process was complete, a color map of the point cloud deviations from nominal was generated, which is shown in Figure 4.9.7. This color map uses color coding displayed on a surface generated on the point cloud to show the deviations from nominal for all areas of the point cloud. Reference geometry (planes, points, lines, circles, cylinder, etc.) can also be created from selected parts of the point cloud data, which is shown in Figure 4.9.8.

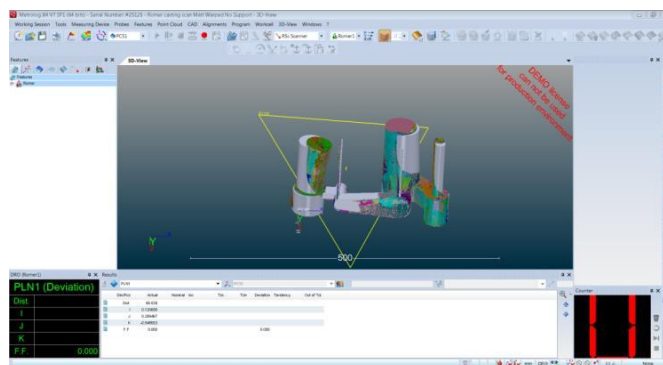


Figure 4.9.6. Nominal solid model and distorted swivel link casting tree point cloud

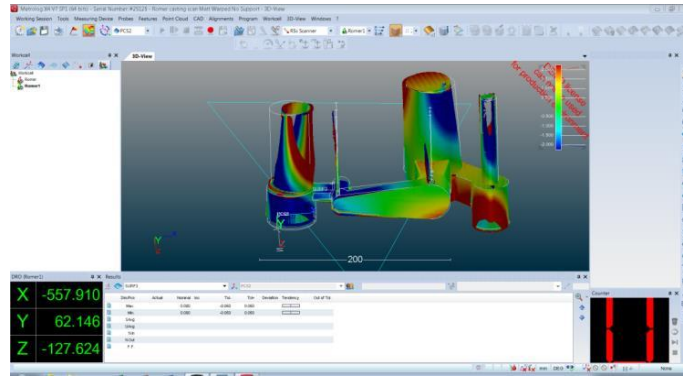


Figure 4.9.7. Color map of point cloud deviations from nominal solid model of swivel link casting tree

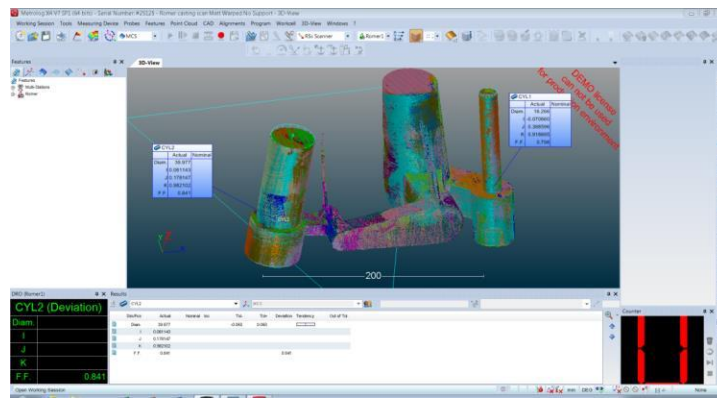


Figure 4.9.8. Creating of reference geometry from point cloud data of swivel link casting tree

As the process of scanning the casting into Metrolog progressed, and as the magnitude of the time required to acquire adequate point cloud data was evaluated, it became apparent that the romer arm was not the appropriate tool for evaluating the casting trees for adaptive machining. It was determined that a robot mounted scanner is a more appropriate tool to evaluate the adaptor arm casting tree for path adapted robotic torch cutting. The casting tree can be positioned in a fixture and an automated robotic scanning sequence used to acquire point cloud data to be used for determining the adapted robotic cutting torch path. A Cobalt Faro Array Imager 5MP was acquired for this purpose. The scanner is compatible with Metrolog software and was mounted on a UR10 robot arm. It provided a low to mid- cost technology demonstration of the geometric adaptive machining algorithm.

Multiple Part Casting Tree

In order to more fully exhibit the capabilities of adaptive machining, GE and WIU-QCML concluded that a multiple part casting tree was required, as the current swivel link casting tree model does not require adaptive machining in order to remove the casting from the tree.

A casting tree design which contains 6 swivel link parts was created. A figure of the newly designed casting tree is shown in Figure 4.9.9.

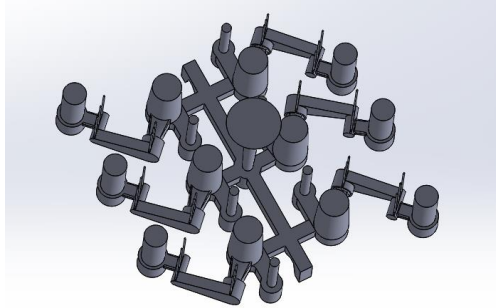


Figure 4.9.9. Image of swivel link casting tree

The locations to be cut by the adaptive machining process are identified in Figure 4.9.10. Cuts 1-12 are required for removing the castings from the tree. Cuts 13-18, although not necessary, will be an excellent test for adaptive machining, especially when the model is distorted. Each of the branches leading to each swivel link casting tree (cuts 13-18) can be independently distorted. A distortion of the branches, by relation, automatically distorts the location of cuts 1-12.

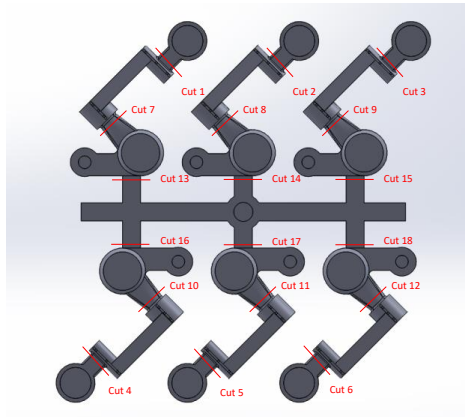


Figure 4.9.10. Swivel link casting tree with robotic cutting locations indicated

The multiple part casting tree model has been scaled by a factor of 0.47459 in order to make 3D printing of the part more feasible. After scaling, the casting tree dimensions are approximately 19.5" X 18.8". In addition to the nominal model which was printed by GE, two different distorted models were designed for 3D printing. Figure 4.9.11 shows the linear offset distortion use case. Figure 4.9.12 and Figure 4.9.13 show the curved distortion use case.

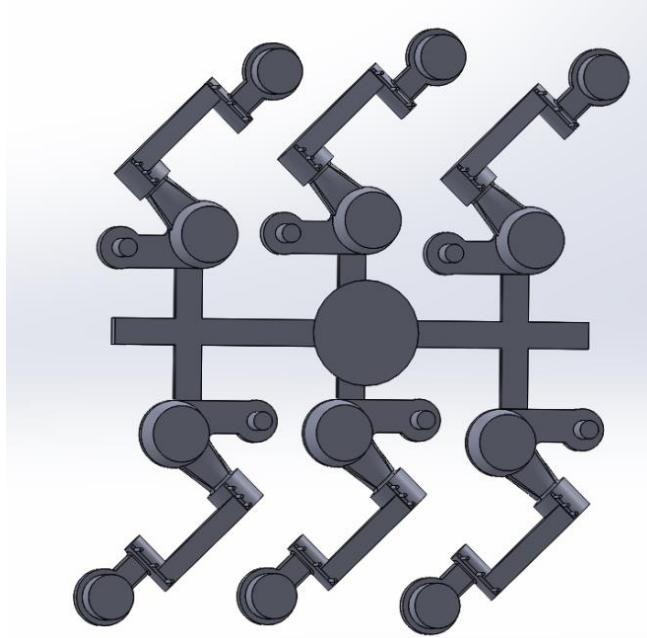


Figure 4.9.11. Image of casting tree with linear offset distortion

Preparations were made to 3D print both distorted models. However, the cost of printing both distorted models was estimated to be nearly \$6000. Consequently, a new combined distortion case was designed which used 3 linear offset swivel links and 3 curved distortion swivel links. Additionally, the funnel shaped riser was removed from the model to reduce the height of the material printed, and the swivel links were removed from the main bus of the casting tree. Printing the casting tree as individual parts increased the ease of 3D printing and the individually printed parts will be glued together afterwards. These revisions in the modeling strategy reduced the cost of 3D printing the new combined distortion case model to \$1120. The figure below shows the newly designed casting tree.



Figure 4.9.12. (left) Top view of casting tree with curved distortion

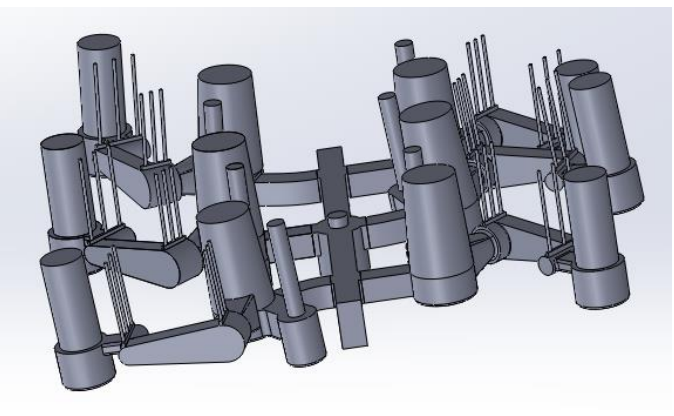


Figure 4.9.13. (right) Side view of casting tree with curved distortion

Programming UR10 Robot in Metrolog

Efforts were continued to utilize the UR10 robot with Metrolog software. We installed V7 of Metrolog, along with i-Robot for use with the UR10 robot. We worked with representatives at Metrologic and Braas (a Universal Robot distributor) to get the UR10 communicating with Metrolog. Many problems arose, and the UR10 robot was upgraded to the software version that was used to develop the Metrolog driver, which is 3.2.20157. Subsequently Service Pack 1 for Metrolog V7 was installed. With this new service pack, it is now possible to control the UR10 robot arm directly from Metrolog. In preparation of receiving the Faro scanner, a model of the Faro scanner was virtually attached as an end effector on the virtual robot in Metrolog. An image of the setup in Metrolog software is shown in Figure 4.9.14.

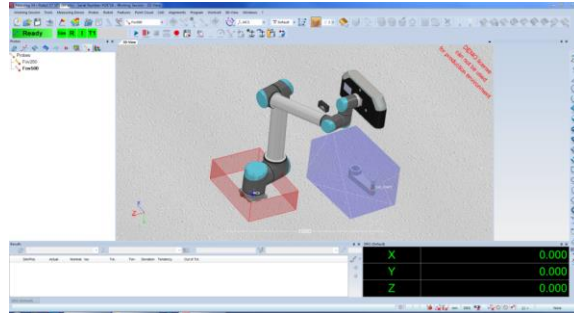


Figure 4.9.14. Simulated Cobalt Faro Array Imager on UR10 Robot in Metrolog

Prior to attaching the Faro scanner, the robot would follow the path commanded in the Metrolog software. However, after virtually attaching the Faro scanner to the virtual robot, the virtual robot would not follow the path commanded in Metrolog. Consequently, a remote service/training session was scheduled with Metrologic representative on May 1, 2017. Once the TCP was manually updated in the UR robot controller, the actual robot followed the path of the virtual robot in Metrolog. A GE robotic engineer had been using a UR robot with an attached Faro scanner. He indicated that robots are not ideal for Metrology due to path following errors. For example, if the point clouds from a robotically positioned Faro scanner are assembled based on the robot positions used for acquisition, the assembled point cloud will have noticeable alignment errors between the point clouds (on the order of 0.0625” -0.125”). The solution is to use optical targets provided with Faro scanner. The targets are placed on or around the part to be scanned such that any of the scans include at least one target from adjacent scans. The positions of the targets can be used to precisely assemble the point clouds. Furthermore, the process of point cloud assembly by targets can be automated.

WIU-QCML developed a Metrolog program that samples point cloud data in predefined locations. A Metrolog program that was created automatically performs the following tasks on a single swivel link casting using the UR10 robot at QCML.

1. Move robot, with Faro scanner attached, to various positions and scan swivel link at each station/location.
2. Detect optical targets at each station/location and automatically align/assemble point clouds into on point cloud.
3. Align assembled point cloud to previously imported swivel link CAD model.
4. Retrieve point cloud data from locations previously defined on the CAD model.

The basic steps of the program were used as a pattern for the program that was developed for the Fanuc 120iC/Faro scanner combinations at Genesis Systems.

Fanuc Robot & Faro Scanner Adaptive Machining Demonstration

Work progressed with the Genesis Systems Fanuc 120iC robot and Faro Scanner as different iterations of a Metrolog program were developed for the nominal multiple part casting tree followed by the distorted multiple part casting tree. A program was developed utilizing the Genesis Systems Fanuc 120iC robot and Faro Scanner that scanned the nominal multiple part casting tree shown in Figure 4.9.15.

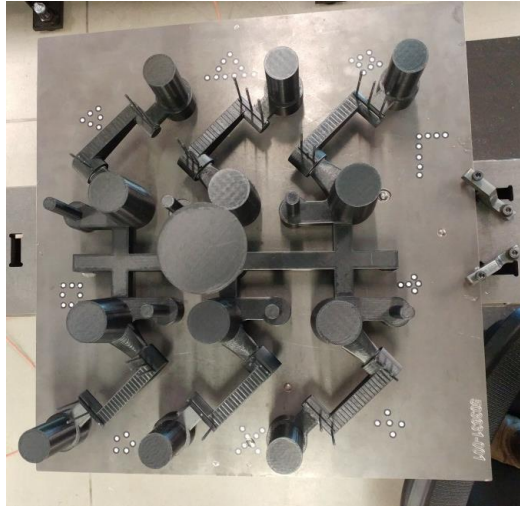


Figure 4.9.15. 3D printed casting tree on platform with optical targets

The program scans the part from multiple surrounding stations (locations) and uses optical targets to align the different point clouds to each other (see white stickers in above image). Autofit is used to align the point cloud to the nominal CAD model as shown in Figure 4.9.16.

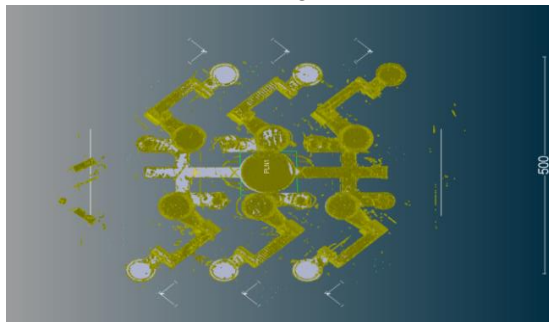


Figure 4.9.16. Screenshot of alignment of point cloud data with solid model

Following Autofit alignment of the point cloud to the CAD model, sections of the point cloud are retrieved based on features defined on the CAD model, as shown in Figure 4.9.17.

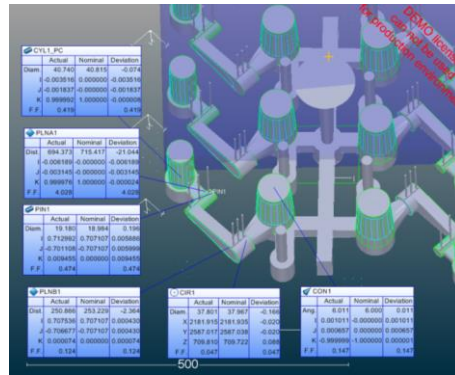


Figure 4.9.17. Metrolog screenshot of feature definition and point cloud retrieval

A distorted casting tree was produced via 3D printing for the development of a Metrolog program, which scans, retrieves, and exports data from the point cloud of a distorted part. The distorted casting tree model used for this purpose has been designed to contain some elements of large distortion in order to test the ability of the Metrolog software to retrieve data corresponding to such large distortions. Figure 4.9.18 shows the point cloud of the distorted part aligned with the nominal CAD model, which clearly demonstrates the degree of distortion designed into the model.

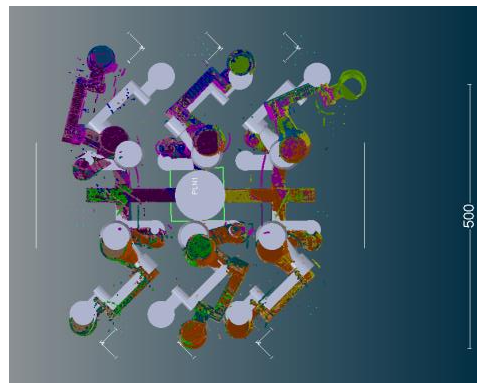


Figure 4.9.18. Metrolog screenshot of alignment of point cloud from distorted casting tree with nominal solid model

After scanning the distorted part from multiple stations, the corresponding point clouds are assembled by use of optical targets. The manner in which the optical targets are used is the same as that shown for the nominal casting tree program (see previous section). In developing the Metrolog program for the distorted part, it was discovered that the Autofit alignment routine could be used to automatically align (no human intervention required) the point cloud to a CAD model for a part with relatively small distortions. However, the distorted part used for this development is far too distorted to use the Autofit alignment routine to automatically align the point cloud. A point pair alignment, which requires human selection of corresponding points on both the CAD model and the point cloud could be used, however, such an alignment cannot be automated for a program.

The only reliable solution discovered for an automated program was to position the distorted part closely to the location of a previously scanned nominal part and recall the autofit alignment known to successfully align the previously scanned nominal part. This procedure will consistently position the point cloud to the CAD model so that the subsequent operation alignment operations can be performed.

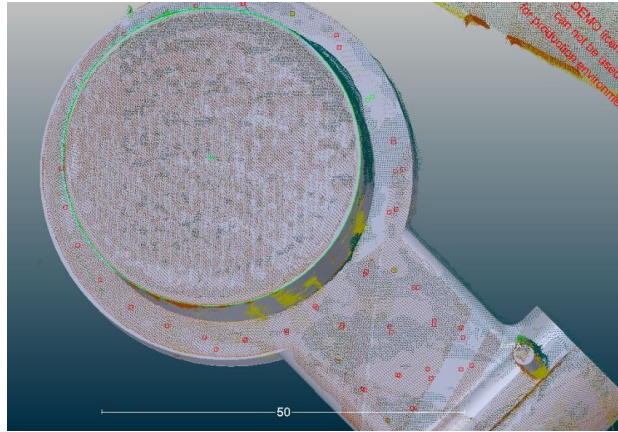


Figure 4.1.21. Screenshot of points generated by a patch on Surface A

Once all of local alignments are performed and the surfaces for data retrieval have been selected, the point cloud is returned to its original alignment orientation and the point cloud data from the selected surfaces is exported in an XyzIjk data format. The exported data is then used in morphing routines for the adaptive machining process.

Metrolog Point Cloud Data Export

WIU-QCML developed various routines to select and export point cloud data from Metrolog. The development process required submission of data to GE engineer, so that he could examine the data, CAD model, and cutting path in external software, and provide feedback. In this process, efforts were specifically focused on exporting point cloud data in the appropriate coordinate system. A discrepancy was observed in the alignment of the CAD model to the exported point cloud data (50-100 mm). Consequently, the CAD model sent to Pinghai was revised such that the CAD origin was oriented in relation to the CAD assembly in the same fashion as the CAD assembly was aligned to RCS in Metrolog. Once the CAD model was created and saved in RCS, the exported point cloud data and the CAD in RCS aligned very well when imported into separate software.

Once the CAD model and the point cloud data were aligned properly when imported into external software, efforts were focused on improving alignment of the cutting path with the point cloud data and CAD. The initial version of the cutting path was created in relation to the actual part. However, it was determined that variation in part location between point cloud acquisition and cutting path creation might introduce error in the location of the cutting path. Consequently, the cutting path was revised such that it was created relative to the virtual CAD model in Metrolog. This new cutting path based on virtual part location/positioning, used in the conjunction with the CAD model in RCS, resulted in the point cloud data, CAD model, and cutting path all being aligned when imported into the external software.

Fabrication of Casting Tree Fixture

There are limitations within Metrolog in being able to perform an autofit of the CAD model to the point cloud. Consequently, the easiest solution is to hold the part in a consistent location by means of a fixture and use a recalled alignment to align the CAD model to the point cloud. The fixture uses a chuck fastened to the fixture plate to grip the cylindrical feature located at the center of the underside of the part. Figure 4.9.22 shows the casting tree in the chuck.



Figure 4.9.22. Image of casting tree fixtured through use of a chuck.

Calibration for Robotic GAM Demonstration

Troubleshooting was performed with Metrolog prior to the robotic AM demonstration. In particular, problems were occurring with establishing tolerance bands that worked consistently for point cloud segmentation/selection. The problem typically was manifested when the part was moved from the location/orientation used to establish the tolerance bands. It was discovered that although the Faro Cobalt scanner was calibrated for image distortion, it is not calibrated for spatial variation. In essence, the scanner was not calibrated to accurately place the acquired point cloud in the position that the part was actually located.

This is typically not an issue because the point cloud data acquired with a Faro Cobalt scanner is used for inspection and/or CAD model generation (reverse engineering). Such operations do not require that the point cloud be accurately placed. The adaptive machining program requires that the point cloud data be accurately positioned or else the derived cutting paths will be in the wrong location. Collaboration between WIU-QCML and Metrologic support engineers resulted in a calibration procedure completely contained within Metrolog.

The calibration process is as follows:

1. A select number of optical targets are scanned with Faro Cobalt
 - a. 3 targets in the “Z” shaped pattern are used.
 - b. The targets are the large purple dots
 - c. The small blue points are the points created from the data acquired from the targets
 - d. The misalignment (calibration issue) is apparent in that the blue points are offset from purple dots shown in Figure 4.9.23.

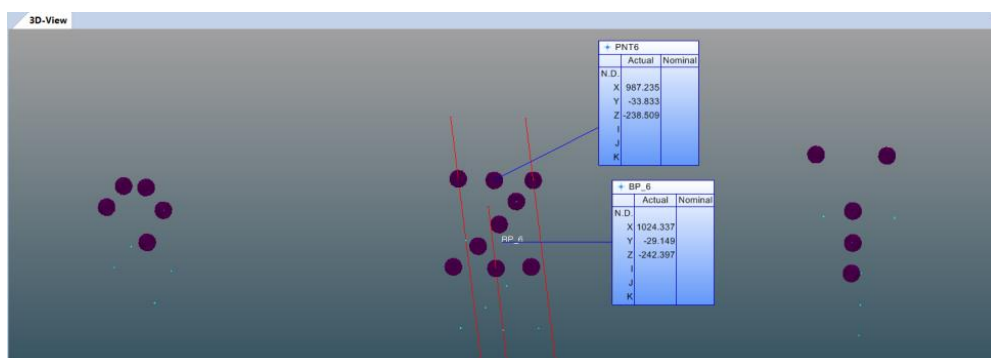


Figure 4.9.23. Quantification of Misalignment

2. A Best Fit alignment is applied in Metrolog to the 3 points
 - a. In the alignment the known X,Y,Z locations of the 3 points are entered into the Metrolog software
 - b. Note: the location of the 3 points was previously measured using an indicator tip on the robot
 - c. The Best Fit alignment shifts the the 3 points to the known X,Y,Z locations
3. The shifted point cloud file containing the 3 shifted points is saved
4. When a new working session is created the shifted point cloud file will be imported before any data is collected
5. As shown in
6. Figure 4.9.24, any data collected will be aligned, by default, with the 3 shifted targets. In other words, the point cloud data acquired will be moved to line up with the 3 shifted points. The shifted points will not be moved.

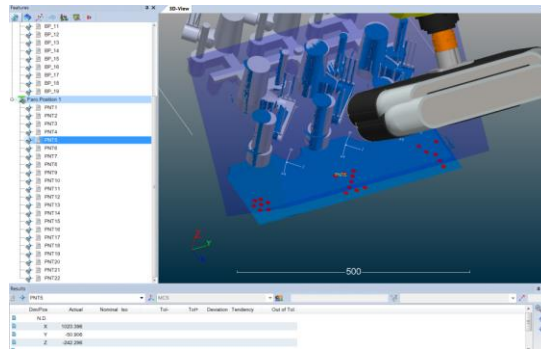


Figure 4.9.24. Automatic alignment of data with three shifted targets.

A calibrated data set was generated from a distorted part and sent to GE. GE used the data set to morph the nominal cutting paths to the distorted part. Once the cutting paths were morphed, validation of the paths was carried out at Genesis. The validation trial showed that the cutting paths followed the distorted part very accurately, thus confirming that the calibration procedure was effective for calibrating the Faro scanner. Efforts were made to reduce the time required to acquire, process, and export point cloud data via Metrolog. A faster laptop computer has been used with the Fanuc robot/Faro system at Genesis. After establishing communication, time study trials showed that the faster computer decreased the required time by 2-3 minutes.

Robotic GAM Demonstration for RIA Casting

A CAD model was required to perform robotic geometric adaptive cutting. However, no CAD model of the RIA casting was available from the arsenal, so time was spent developing a CAD model for the casting. Once work to model the casting was completed, the castings were transported to Genesis Systems. A vice was positioned in front of the robot as a work holding fixture. Once the position of the work holding vice was known relative to the robot coordinate system (RCS), the CAD model of the RIA casting was moved into RCS, such that coordinate system of the CAD model matched the RCS.

A Victor MT310 machine torch was purchased from Praxair. The MT310 is a three hose torch which would allow for independent control of acetylene, the preheat oxygen, and the cutting oxygen. Two oxygen regulators, one acetylene regulator, cutting tips, a tee for the oxygen, an auxiliary oxygen valve, and three 25' hoses (one acetylene and two oxygen) were also purchased from Praxair.

An adaptor to hold the machine torch as an end effector on the robot was designed and fabricated. The adaptor was designed to use an air powered automatic tool change coupling provided by Genesis. The coupling will allow for quick change over between the Faro scanner and the oxy-acetylene torch. The design of an ignition system for the oxy-acetylene torch was also researched and purchased. These included a 120 VAC momentary contact switch, a spark plug and spark plug cable, an electrical cord, and an AC ignition transformer.

A Metrolog program was created and refined to scan the RIA casting, perform the necessary best fits, and export the relevant data. The RIA casting was scanned in an inverted position while being held in the vice. Issues were encountered in getting the RIA casting CAD model to appropriately best fit to the point cloud data. It was determined that the best fit issues stemmed from the CAD model not matching the point cloud data because only the top of the casting (the side facing up while being held in the vice) was scanned. This issue was resolved by truncating the CAD model so that it had more correlation to the point cloud. In addition to a Metrolog program which scans, fits, and exports data, a technique was developed for executing the GE morphing tool from Metrolog. The approach utilized the “SPAWN” command to call and execute the morphing tool.

After the torch and ignition system were set up, time was spent running development trials to validate recommended cuttings parameters for 3” thick steel. The trials confirmed that the cutting parameters recommended by the torch manufacturer were capable of cutting 3” thick steel. Dry runs were performed to evaluate morphed cutting paths. Some issues were encountered with the cutting paths, so time was spent communicating with GE (Pinghai and Mohammed) to diagnose the issues. An issue was encountered with the cutting path indicated in red in the image shown below. The surface highlighted in blue was the point cloud data used for the morphing operation. It was determined that the issue was caused by the exported data being contained in a single plane (the blue surface shown in Figure 4.9.25).

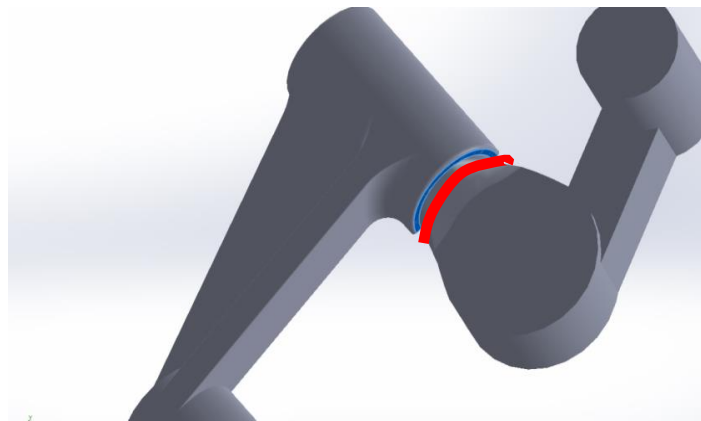


Figure 4.9.25. Image of solid model showing exported data in single plane.

The problem with extracting and exporting data from a single plane is related to how the morphing tool calculates and performs morphing. The morphing tool will only adjust in the direction in which a deviation is reported. For example, if deviations are reported only along the x-axis then the correction/morphing will only be made along the x-axis. As an alternative to the exported surface shown in Figure 4.9.25, the adjacent surface was used for data export, as shown in Figure 4.9.26. Once this change was made, the morphing results improved. Errors were also found and corrected in the cutting paths, which yielded further improvements in the morphing results observed in the dry run tests.

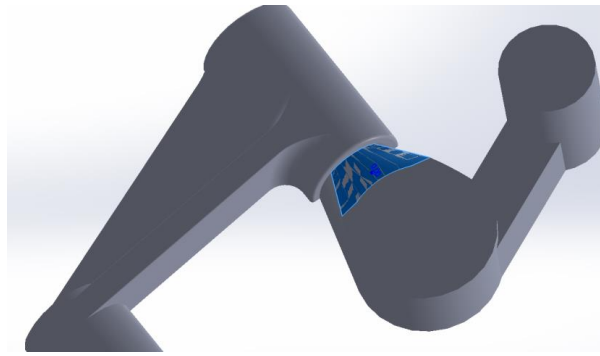


Figure 4.9.26. Image of solid model showing revised surface for data export

The oxy-acetylene torching cutting demo was carried out on March 19, 2018 at Genesis Systems Group at 11:00 am. There were some issues with residual sand on the surface of the castings interfering with the preheating and initialization of the cutting process. However, once the sand was removed (both by chipping and grinding) the preheating and cutting processes worked properly. The demonstration videos of the robotic adaptive torch cutting of the adaptor arm were analyzed to determine the time required for each step of the adaptive cutting process, and the resultant time was compared to the time reported by the RIA using current manufacturing methods. The table below reports the results of the analysis.

Robotic Adaptive Torch Cutting of Adaptor Arm Casting		
Step in Process	Time Required (min)	Comment
Load part in fixture	1	
Scanning	1	
Metrolog Processing/Morphing	.333	
Conversion of morphed LS to TP file	1	This step would not be required in production if the robot were configured to read LS files
Tool Change	1	This step could be eliminated. Mount torch and scanner on same rotating adapter.
Upload TP file to robot controller	1	
Torch Ignition & Positioning	.5	
Preheat #1	1	An estimate of the required preheat time was determined by measuring the elapsed time after the torch was successfully position for preheat
Cut #1	0.333	
Preheat #2	1	An estimate of the required preheat time was determined by measuring the elapsed time after the torch was successfully position for preheat
Cut #2	.5	
Total Time (min)		
8.6667		
RIA Band Saw Cutting of Adapter Arm Casting		

Step in Process	Time Required (min)	Comment
Cutting on band saw	18	
Comparison of Robotic Adaptive Cutting to RIA Band Saw Cutting		
Robotic Time (min)	RIA Time (min)	% Reduction in Time Using Robotic Adaptive Cutting
8.6667	18	51.9

In production of the adapter arm, the RIA currently uses manual labor to band saw cut the gates and risers from the casting, which requires 18 minutes per casting. In contrast, the robotic adaptive torch cutting requires 8.667 minutes, which is a 51.9% reduction in cutting time when compared to the RIA band saw cutting. The time required for robotic adaptive torch cutting could be further reduced by eliminating the need for LS to TP file conversion and eliminating the need for a tool change by mounting the scanner and the torch simultaneously on the same rotating adapter. If those two steps were eliminated the required time would be reduced to 6.667 minutes, which is a 63.0% reduction in cutting time when compared to the RIA band saw cutting. Certainly other time saving measures could be implemented, as well, making robotic adaptive cutting even more attractive. In summary, this time study shows that robotic adaptive torch cutting is a viable way to reduce to time required for cutting unnecessary parts from castings or other similar parts. If the selected parts are produced in sufficient quantities to justify the capital investment, robotic adaptive machining can be an attractive way to reduce time and costs.

Revision to Distorted Swivel Link Casting Tree Design

In order to further develop the robotic GAM process, it was decided that the design of the distorted swivel link casting tree should be revised due to issues stemming from the large distortions present in the original design. The design process included reviewing the methodology and approach of the original nominal and distorted casting trees, design swivel links with local distortions, and assemble the distorted swivel links onto the casting tree. Once the reduced distortion casting tree CAD model was completed, a ParaSolid version of the model was sent to Pinghai for point cloud generated based on the CAD geometry.

The reduced distortion casting tree is quite similar in design to the original distorted casting tree, as shown in Figure 4.9.27.

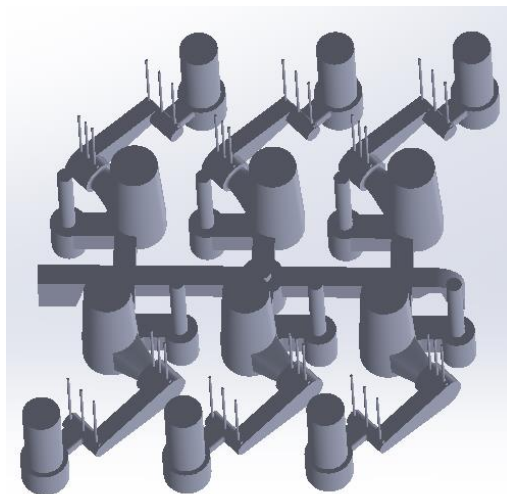


Figure 4.9.27. Reduced distortion casting tree solid model

Instead of the large global distortions that were used in the original distorted casting tree, the reduced distortion casting tree utilized smaller localized distortions. The reduced distortion casting tree incorporates local distortions on four of the six parts. Two of the locally distorted parts have +/- variation along the length, where one has - variation and the other has + variation. The other two locally distorted parts have +/- variation along the shoulder, where one has - variation and the other has + variation. The other two parts are nominal. The image below shows the distorted and nominal parts labeled on the casting tree. Figure 4.9.28 describes the nature of the distortion for each part on the casting tree.

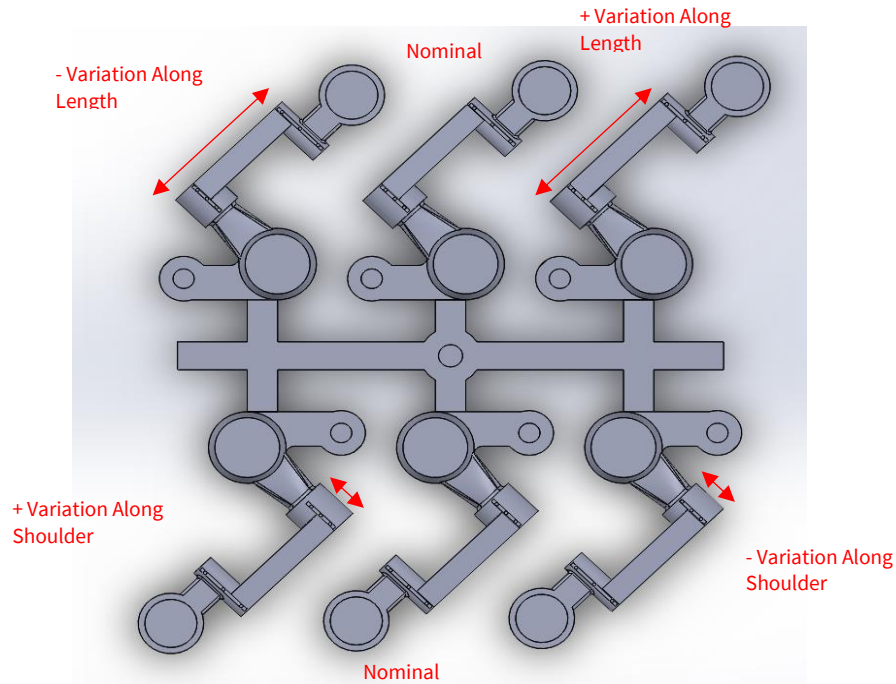


Figure 4.9.28. Description of distortion on casting tree

Once the reduced distortion casting tree CAD model was complete, time was spent learning how to use the virtual cobalt scanner to generate a point cloud with sufficient point density for data extraction/export. Evaluation trials indicated that Metrolog is able to auto-fit the nominal CAD model to point cloud generated from the reduced distortion CAD model. This was a significant step because it was not possible with the original distorted casting tree due to the large global distortions. Subsequent trials were used to ensure that the auto-fit will work with the nominal CAD model in various positions relative to the virtual point cloud. Once satisfactory results were obtained for a variety of orientations, the program was fully developed to perform local fits and extract/export data and transformation matrices. In order to move the next planned step of actual point cloud acquisition, the reduced distortion casting tree would need to be 3D printed. Due to the time required to 3D print the reduced distortion casting tree and based on the success of the virtual trials, it was decided to bypass the step of 3D printing the reduced distortion casting tree and incorporate the design into the sheet metal casting tree.

Sheet Metal Reduced Distortion Casting Tree

The reduced distortion casting tree was used to design the sheet metal casting tree. The outline of the top view of the reduced distortion casting tree (see top view shown in previous figure) was projected onto a sketch plane and extruded to the thickness of the sheet metal to be used, as shown in Figure 4.9.29. A

hole in the center of the part was included in the design for the purpose of fixturing the part with threaded rod and jam nuts.

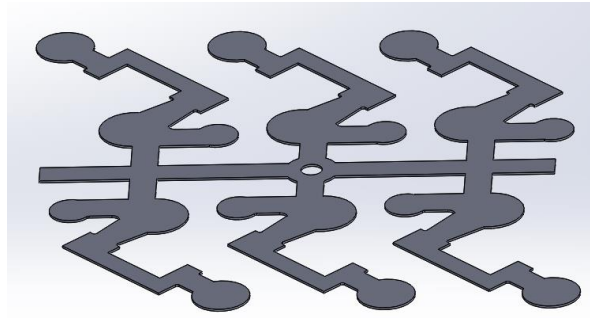


Figure 4.9.29. Image of solid model of sheet metal reduced distortion casting tree

Given that the 3D printed reduced distortion casting tree cannot be cut with a plasma cutter, the sheet metal design was created so that a representation of the reduced distortion casting tree could be cut with the plasma cutter for demonstration purposes. The 14 gauge sheet metal for the sheet metal reduced distortion casting tree was purchased from Rich Metals Co. in Davenport, IA. Six sheet metal reduced distortion casting tree parts were produced as shown in Figure 4.9.30.

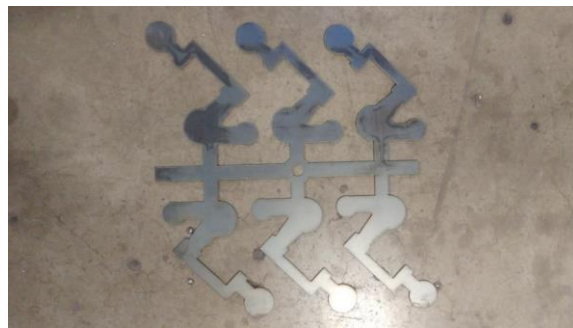


Figure 4.9.30. Image of fabricated sheet metal reduced distortion casting tree

The fixture for holding the sheet metal casting tree was assembled in the robot cell. The Metrolog program for scanning the sheet metal casting tree was also developed. Figure 4.9.31 is an image of the sheet metal casting tree undergoing the scanning process.

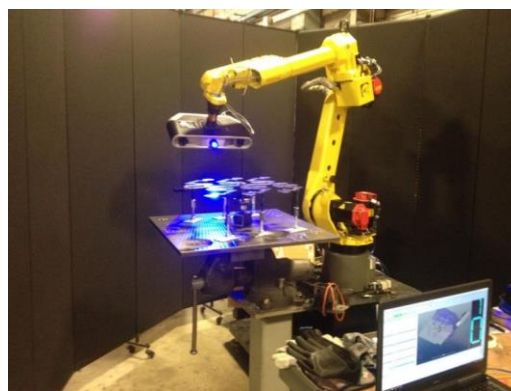


Figure 4.9.31. Scanning of sheet metal casting tree

Data collected by the scanning process was exported and used to morph the cutting paths. The morphed cutting paths were very close to the actual part, but small discrepancies were observed. Analysis of the results and consultation with the GE robotic GAM team suggested that the observed discrepancies were due to the use of only one local fit and the resulting correlation error. Put differently, using one local fit only aligns the CAD model to the point cloud in a local region, while the rest of the CAD model does not align with the point cloud. This accounts for some of the cutting paths matching parts, while other cutting paths showed varying discrepancies from the scanned part. Based on this analysis, it was concluded that two local fits would need to be used on each part of the sheet metal casting tree, as shown in Figure 4.9.32.

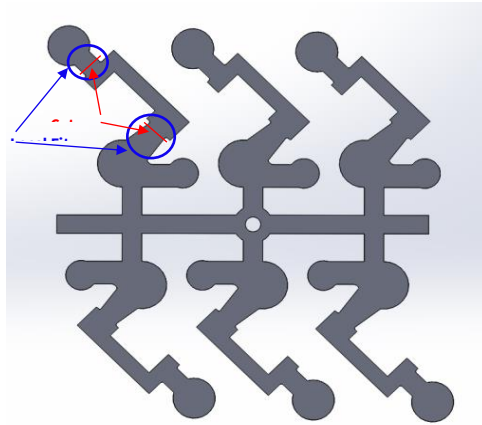


Figure 4.9.32. The two regions in which the local fits are applied to each part on the casting tree

After the two local fits were applied to each part of the casting tree, the morphed cutting paths matched the actual part very well. With everything working, the plasma cutter demonstration on the sheet metal casting tree was held on April 19, 2018 at Genesis Systems Group. Figure 4.9.33-Figure 4.9.43 were taken during the demonstration.

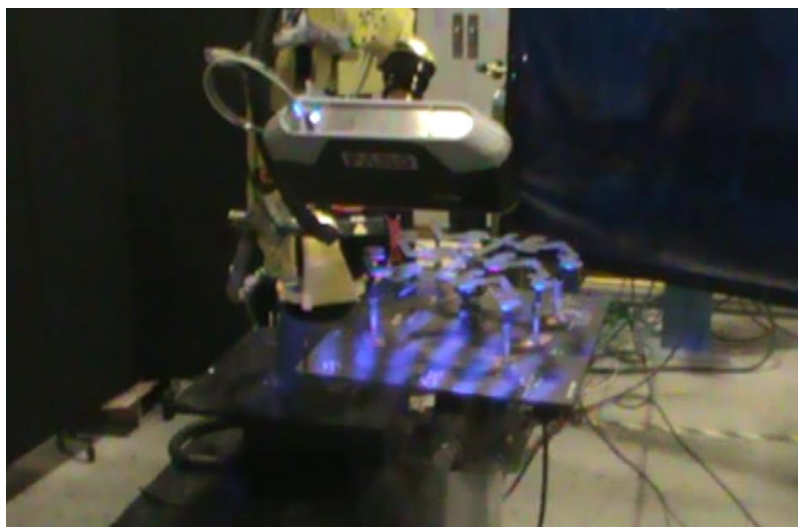


Figure 4.9.33. Scanning of the casting tree with Fanuc robot and Faro scanner.

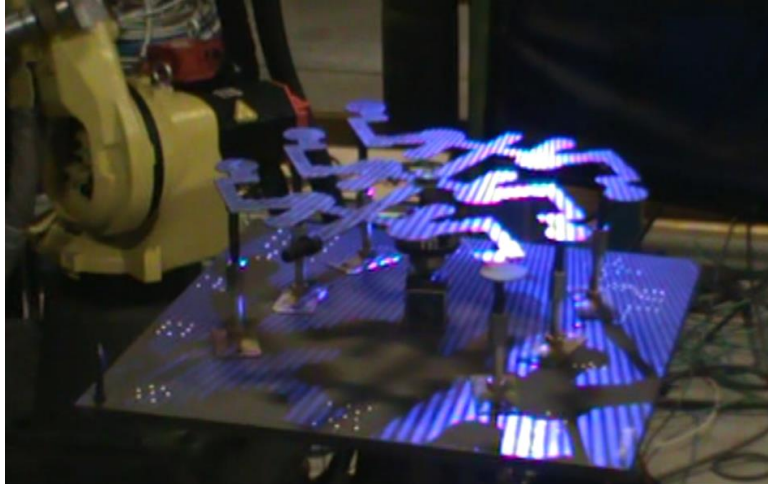


Figure 4.9.34. Close-up view of scanning the casting tree.

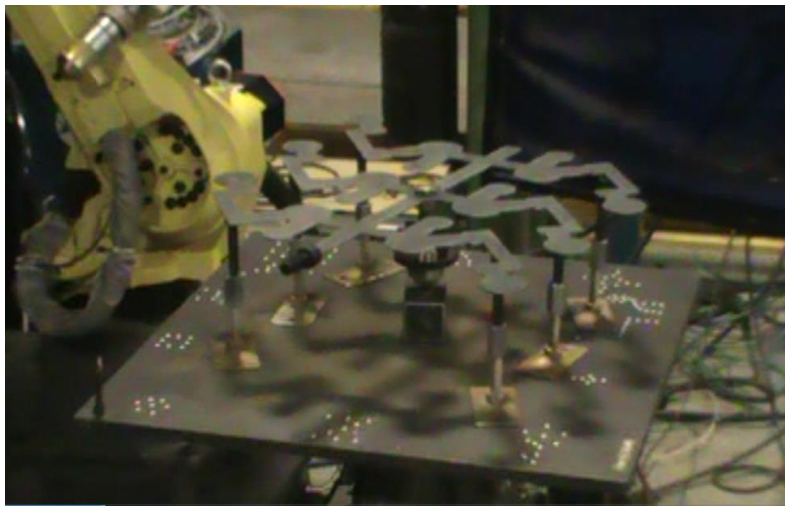


Figure 4.9.35. An image of the casting tree after scanning and prior to morphing & cutting.

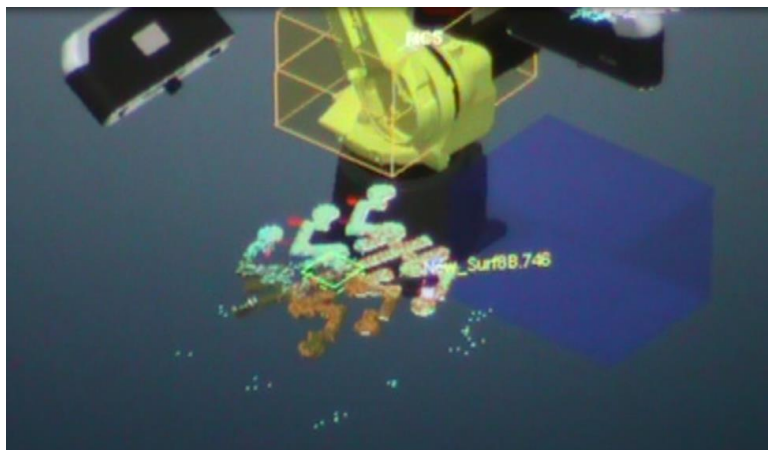


Figure 4.9.36. An image of the Metrolog interface performing autofits to the point cloud data and data extraction/export

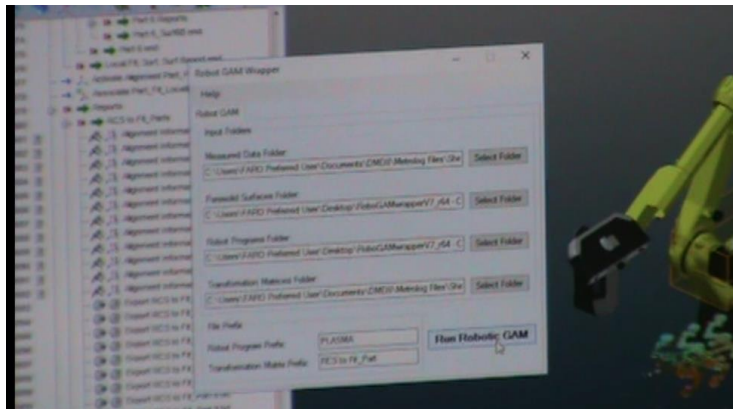


Figure 4.9.37. An image of the GE RoboGAM app being launched by the Metrolog program.



Figure 4.9.38. An image of the plasma cutting torch at the first cut location on the casting tree.

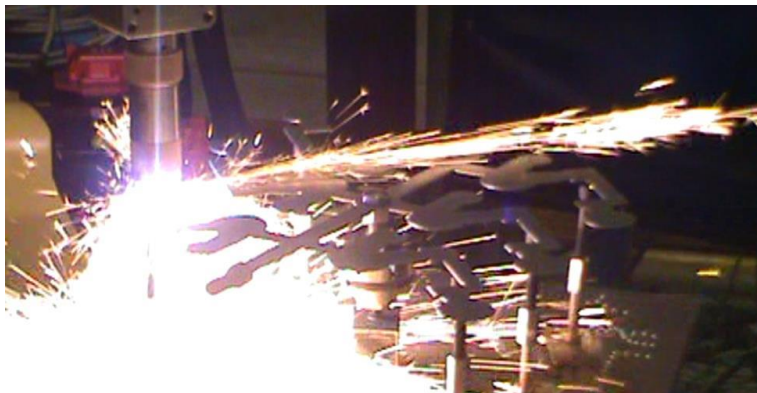


Figure 4.9.39. An image of the of plasma cutting torch in operation at the first cut location on the casting tree.



Figure 4.9.40. An image of the cutting torch at a subsequent cut location.

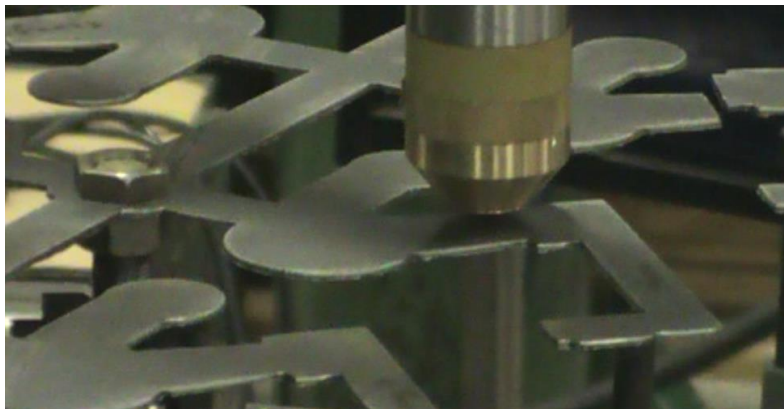


Figure 4.9.41. An image of the plasma cutting torch at a subsequent location. In this image locations that were previously cut can be seen.

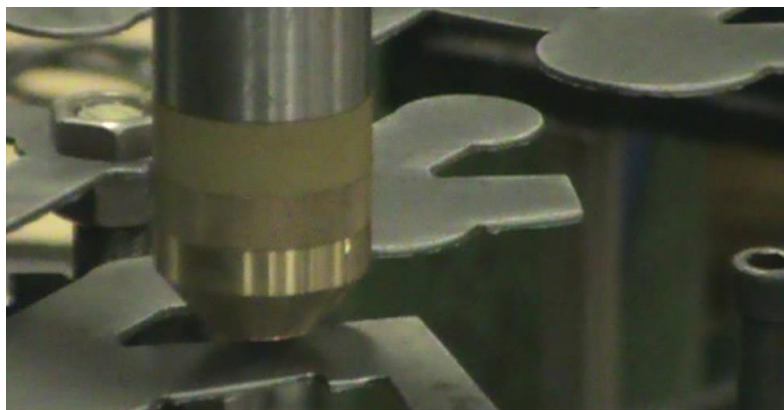


Figure 4.9.42. An image of the plasma cutting torch at the last cutting location. Once again, in this image locations that were previously cut can be seen.

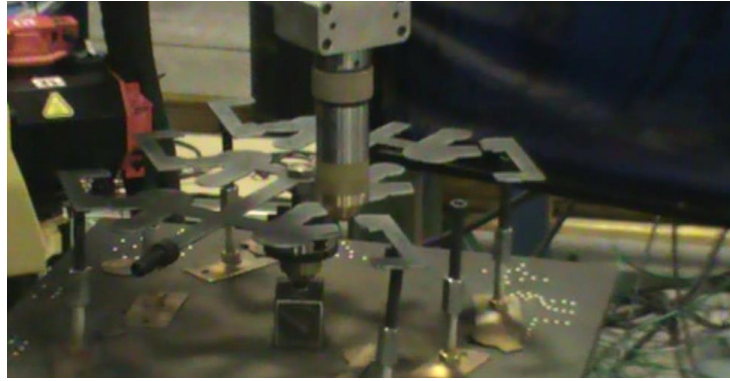


Figure 4.9.43. An image of the plasma cutting torch above the final cut location after the execution of the cutting operation. All programmed cuts have been performed in image.

Mill GAM

There were four demonstration use cases for GAM with a mill, which included airfoils (GE), swivel link (simulated RIA), an impeller (blind use case), and clamping bracket (simulated RIA). Demonstrations were performed on a Haas mill at WIU. A touch probe was ordered and installed in the mill as shown in Figure 4.9.44 and Figure 4.9.45.



Figure 4.9.44. (left) Probe setup in Haas mill at WIU
Figure 4.9.45. (right) Close-up of probe mounted in Haas mill

Once communication was established, we were able to move forward with utilizing the Renishaw OMP 40-2 probe in conjunction with the mill. Our purpose in using this probe is to take measurements of parts and produce deviation data, which will be input into the GE morphing algorithm. There are two major types of probing macros available for call out in a CNC program: linear (P9811) and angular (P9821). The linear probing macro commands the probe to move to a specified location in the x or y direction from a starting position until the probe is triggered by contact with the part. The probe will actually move a small distance past its specified distance to account for a reasonable amount of deviation. When probing linearly, the machine only prints deviation data in the direction that it moved to take the measurement. In other words, if the probe moves in the x direction to take its measurement, it only prints the deviation between the measured x coordinate and the nominal x coordinate. Therefore, when deviations in x and y directions are required, two separate probe measurements must be taken for each point. A small number of the provided xyz coordinate points could best be probed linearly in one direction, but not the other, making accurate measurements challenging. Another issue with linear probing is that it is highly inaccurate when attempting to measure angled surfaces. The use of angular probing is often the better option in this case.

Angular probing commands the probe to move along a specified angle to a specified distance from the starting position until the probe is triggered by contact with the part. The probe will move a small distance past its specified distance to account for a reasonable amount of deviation. When probing angularly, the machine prints deviation data for both the x and y coordinates, as well as relating to the distance specified by the program. This can potentially reduce the amount of measurements to be taken depending on the geometry of the part, as only one probe measurement is required to produce deviations in both x and y directions. To produce the most accurate results, this type of probing should be used on flat surfaces, and the probe path from the starting position should be along a direction normal from the surface.

Two programs have been created to carry out probing of our models. The first program utilizes all linear probing commands, and the second program utilizes all angular probing commands. The deviation results between these two programs are inconsistent, as a result of high amounts of error in the probe measurements. We have determined that for a vast majority of the probe points, linear probing is highly inaccurate and should be avoided.

It is worth noting that neither linear nor angular probing works well with contoured surfaces. The probe expects to contact the part at a point which lands on the line of motion and is coincident with the center of the probe. When probing a convex surface, this is often not the case, and it is difficult to quantify how far off the contact point is without extensive offline calculations. Angular probing could possibly be used in the case of convex surfaces, but the angle of a line normal to a line tangent to the surface, and coincident with a specified point, must be known for this type of probing to be accurate. Again, this would take a significant amount of offline calculation and/or in-depth and time consuming programming.

There are some limitations of the Renishaw OMP 40-2 probe. This probe model is triggered when one or more of three internal electrical contacts are broken. Therefore, it can only be accurately calibrated at 30 degree increments. Consequently, angular probing at angles not at these 30 degree increments will involve a considerable amount of error.

Airfoils (GE)

General Electric (GE) supplied QCML with a parasolid file representing the nominal dimensions of a simulated GE airfoil, as well as a text file which provided the xyz coordinate points to be probed for measurement. It was desired that we could produce measured deviations of a distorted 3D printed model

from the nominal probe points. The best results are produced probing the flatter side of the airfoil using the angular method. The deviations fell within an acceptable range as defined by GE. However, when probing the convex side of the airfoil, we see deviations on the order of 0.250", which was unacceptable.

The first angular probing programs used probing paths at an angle of 45 degrees relative to the coordinate system. While this program seemed to offer better and more consistent results than the linear probing program, we decided the accuracy could be improved upon. It was determined that probe paths at an angle normal to a line tangent to the surface of the part and coincident with the provided probe point would ensure that the probe contacts the surface with a higher degree of accuracy. Using SolidWorks software and the airfoil parasolid file provided by GE, we were able to geometrically calculate the necessary information to produce a program that uses calculated angles and starting positions for each individual probe point. It is worth noting that this process was rather tedious and time consuming. The program was then tested by being implemented upon a nominally dimensioned 3D printed model, and the deviation data fell within the tolerances of our 3D printer's capabilities.

Extensive amounts of probing tests were conducted on both distorted and nominal models. This was done to try and see if our probing program produced deviation data that represented the intended distortions of the airfoil model. Unfortunately, some of our distorted model deviation data fell outside of the tolerances as verbally indicated by GE engineer, even though our probing of the nominal model yielded acceptable results. We believe this to be due to poor printing resolution, part-loading errors, or zeroing errors. Because of the inaccuracies of our distorted model probing data, we conducted further testing involving removing and re-loading parts, as well as re-zeroing the probe, to try and quantify any error during work-holding and/or zeroing the probe. We learned that the data can vary to a somewhat significant degree, leading us to believe the procedure involves some repeatability errors.

Applied Automation Technologies (AAT3D) came to WIU to demonstrate their software package called Computer Aided Part Programming Software NC (CAPPSNC). Using their software, AAT3D was able to generate probe points on the airfoil CAD model that we have been working with. In the same program, they generated the CNC code to carry out the probing operation in our mill and collected the deviation data. This data was then able to run through GAM algorithm in order to morph the CNC code to compensate for the deviations from the distortion of our 3D printed models. The models were then machined, yielding exceptional results showing that the machining process was adapted to allot for the distortion measured by the probe.

Several distorted models of these airfoil section arrays made of ABS plastic, as well as one made of 4047 aluminum were 3D printed in order to test our probing programs. Image of the polymer airfoils are shown in Figure 4.9.46 and Figure 4.9.47. Images of the 4047 aluminum airfoils are shown in Figure 48 and Figure 49. The probing programs were written using constraints provided by GE in the form of xyz coordinate points from the nominal dimensions of the part. The physical geometry of the airfoil section array also presented constraints that needed to be considered when establishing the probe paths.

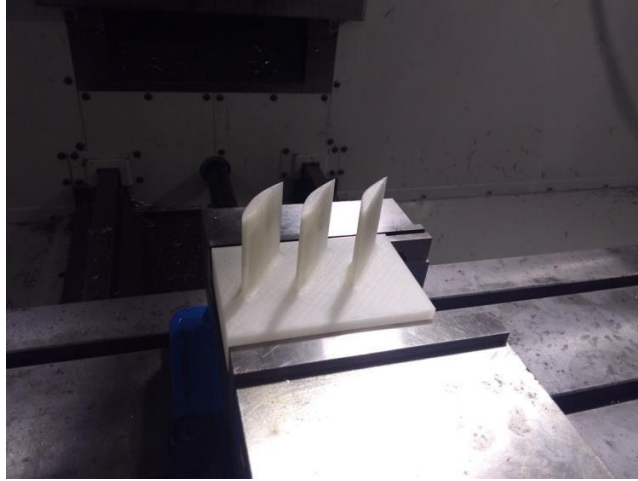


Figure 4.9.46. Plastic printed airfoils for milling demonstration

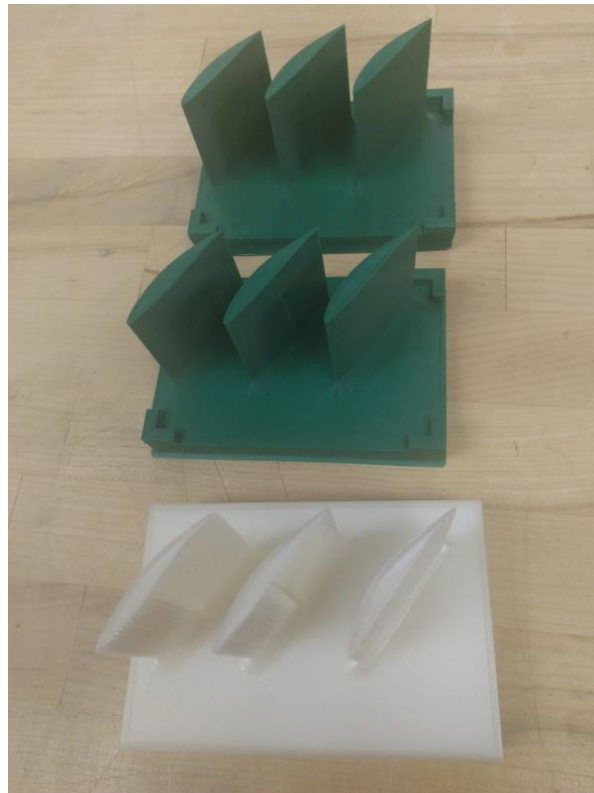


Figure 4.9.47. Plastic printed airfoils for milling demonstration



Figure 48. Image of 3D printed aluminum airfoils

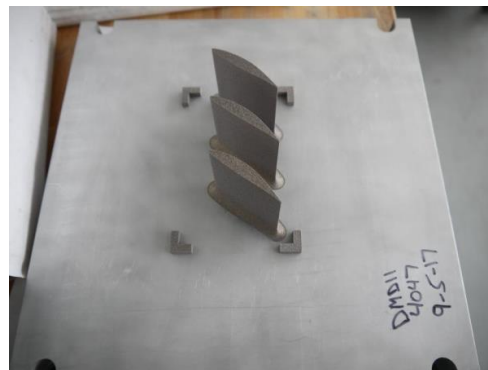


Figure 49. Image of 3D metal printed aluminum airfoils

Swivel Link (Simulated RIA)

A meeting was held with Rock Island Arsenal and an adaptor arm was identified as a potential use case. RIA indicated that the solid models of this part could not be shared with foreign nationals. In order to deal with this issue, we identified the critical features present on the part that the adaptive machining software algorithm would need to identify. We then created a solid model of an entirely new part that is geometrically and dimensionally different from the files provide to us. An image of the simulated adaptor arm (swivel link) solid model is shown in Figure 50.

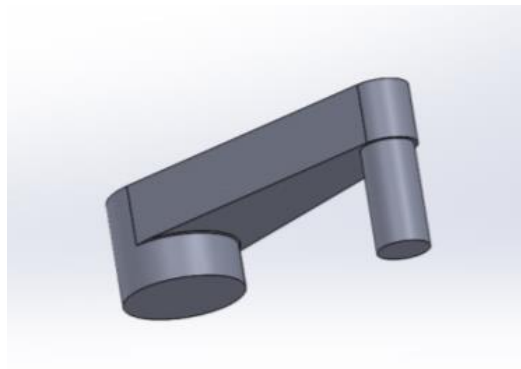


Figure 50. Solid model of simulated adaptor arm (swivel link)

The swivel link is a casting which is produced on a casting tree. This casting requires post process machining to achieve desired dimensions. After some consideration, it was decided that machining swivel link models from aluminum stock would better produce a machinable model while keeping material and labor costs as low as possible. It was also decided that ½” of rectangular stock would be left on the bottom of the part to allow for work-holding in a standard mill vise.

Tool paths based on nominal final dimensions of the desired features for the swivel link were produced. These tool paths were used with GE’s software to morph and generate adapted CNC code that factors in part distortions. The pin and the bore of the swivel link (indicated in Figure 4.9.51 as “Surfaces to be probed”) would be probed independently and the cutting paths morphed independently.

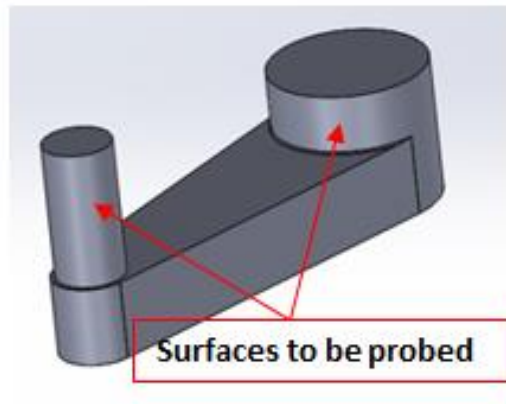


Figure 4.9.51. Surfaces to be probed on the Swivel link

The CAM programming to produce the swivel link models was completed and three models were successfully produced to be used in probing and adaptive machining trials and demonstrations. As shown below, part of the rectangular block was left as a surface to clamp in the vice. An image of the fabricated swivel link and the solid model of the swivel link is shown in Figure 4.9.52.

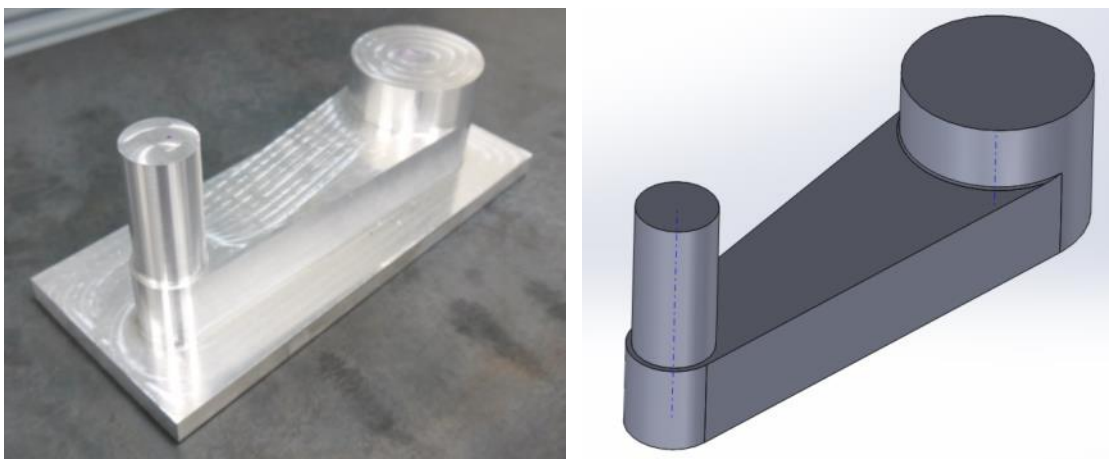


Figure 4.9.52. Image of fabricated swivel link (left) and solid model of swivel link (right)

Several steps in the CNC GAM process require a nominal CAD model that has a coordinate system that corresponds to that of the mill on which the probing and milling will take place. To achieve this for the

swivel link, the swivel link was probed with a Romer arm to determine the orientation of the coordinate system of the HAAS TM-3 mill relative to the swivel link features once the part is clamped in the vice for machining. The coordinate system of the CAD model for the raw (unmachined) swivel link, shown in Figure 4.9.53, was shifted to correspond with that of the HAAS TM-3 mill consistent with the results of the Romer arm evaluation. The figures below show the coordinate system before and after the coordinate system change, shown in Figure 4.9.54 .



Figure 4.9.53. Image of coordinate system before alignment with Haas mill

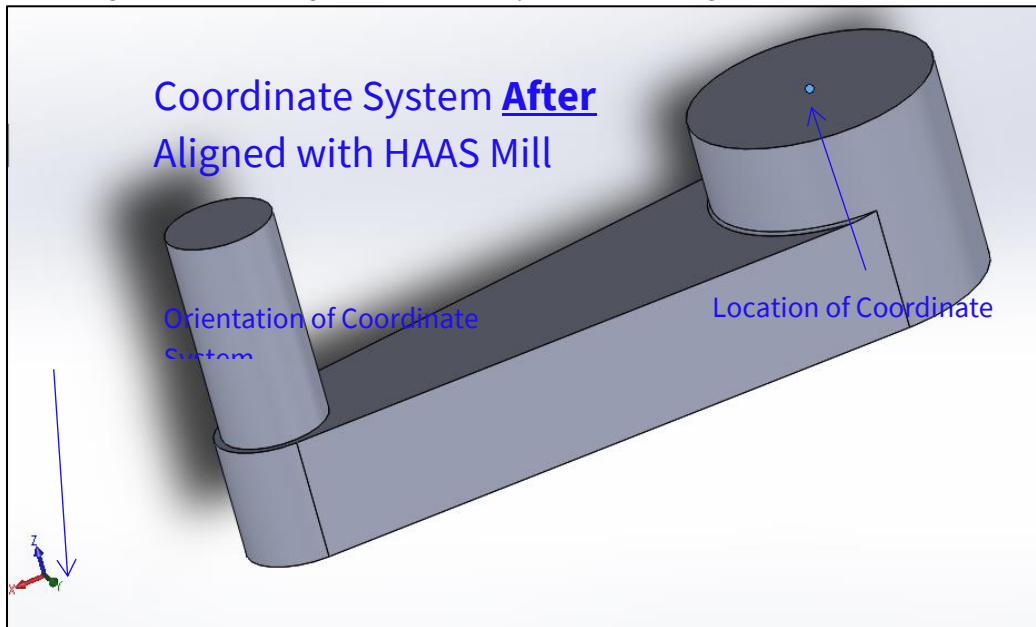


Figure 4.9.54. Image of coordinate system after alignment with Haas mill

The most notable change that bears mentioning is that two separate and independent DMIS programs were developed for the pin and the bore. This allowed the morphing to be applied stepwise, first on the bore, which did not require morphing because it was centered on the part origin, and second on the pin. The morphing shifts the CNC tool path for the pin to the distorted location of the pin on the probe part. Probing was performed on 2 of the 3 swivel links to determine the spacing between pin and the bore. The location data was analyzed so that it could be compared to post machining measurements of the swivel links in order to evaluate the effectiveness of the GAM process.

The CAD model of the swivel link is shown to the right. The nominal distance between the pin and the bore features is 201.17 mm. Aluminum swivel links were designed and manufactured to have 1.59 mm positive distortion (1/16" or 0.0625 in). This results in a distance of 202.76 mm between the pin and the bore features. The distorted aluminum swivel link was set up on the HAAS TM-3 mill and the pin and bore features were measured using a Renishaw probe. An image of the probing taking place on the HAAS mill is shown in Figure 4.9.55. As reported previously, the probing and morphing of the pin and bore were performed separately and independently.



Figure 4.9.55. Imaging of probing being performed on Haas mill

Once the probing was complete, the data was compiled, compared to the nominal CAD surfaces, and the corresponding cutting paths were morphed accordingly. The morphed cutting paths were uploaded to the HAAS mill and the swivel link was milled, as shown in Figure 4.9.56.



Figure 4.9.56. Milling of swivel link

An image of the finished swivel link is shown in Figure 4.9.57. The image also displays a representation of where the nominal cutting path is located relative to the distorted part and the direction in which the cutting path was morphed. As reported previously, the bore is centered on the origin of the part which is located at the center of the large diameter bore stock. Consequently, no morphing of the cutting path is required for the bore. The image also shows a small amount of the original pin material left at the base of the machined pin. This original diameter material was left to evaluate the location of the machined pin relative to the pin. The romer arm was used to probe the surfaces of the pin and original diameter

material at the base of the pin on each part. The results of the evaluation are given in the table following Figure 4.9.57. The results of the evaluation show that the morphing placed the location of the cutting path within less than 0.2 mm (0.008 in) of the original probed material.

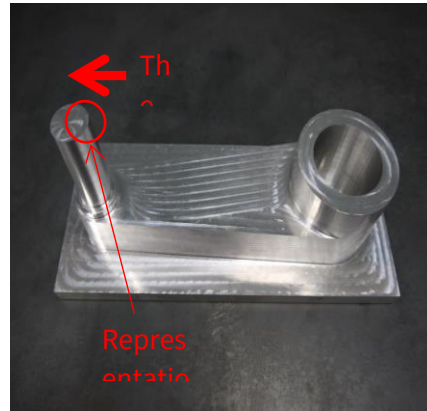


Figure 4.9.57. Image of milled swivel link

Romer Arm Evaluation of Morphed Locations of Machined Swivel Link Pins	
Swivel Link ID	Center to Center Distance Between Pin and Original Material (mm)
Swivel Link_1	0.131
Swivel Link_2	0.196
Swivel Link_3	0.133

A demonstration of the probing, morphing and milling of the swivel link for Rock Island Arsenal was scheduled on Thursday, June 21, 2018. The demonstration was attended by Dan Hanson, Ed Flinn, and Randl Besse from RIA.

Impeller (Blind Use Case)

A 3D printed impeller was designed as the blind use case. Features on the impeller will require that it be oriented at a 45° angle so that internal support structure can be eliminated. The 45° orientation will require a substantial amount of support structure underneath part. However, the underside of the part has cutaway features that will be filled with support structure material. The printed parts will be probed and adaptive machining will be used to remove the support structure and cleanout the cutaway features filled with support structure material. Images of the impeller and the impeller with support structure are shown below in Figure 4.9.58-Figure 4.9.60.

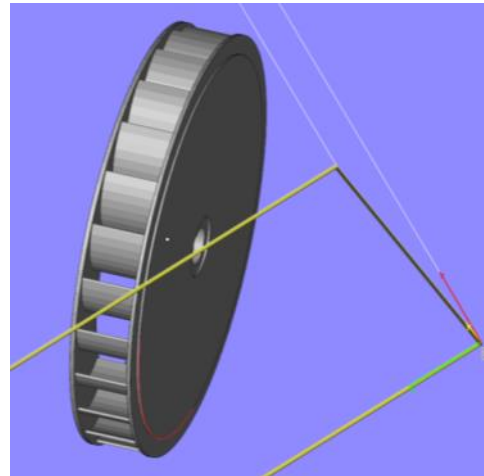
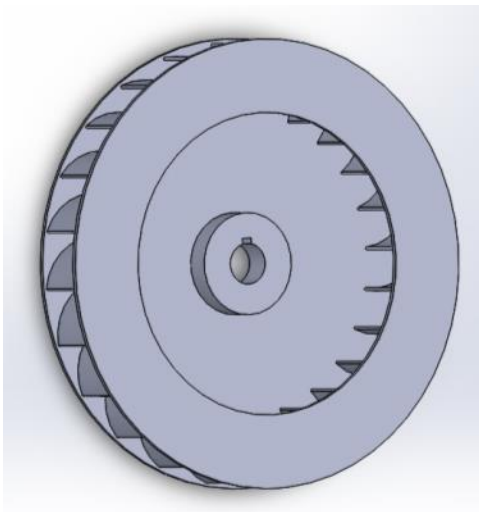


Figure 4.9.58. Impeller top-view (left)
Figure 4.9.59. Impeller side-view (right)

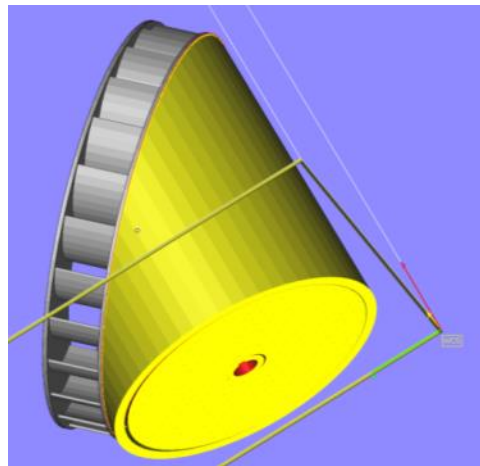


Figure 4.9.60. Impeller side-view with support structure

The impeller was 3D printed in 4047 Al in the EOS system utilizing support structure, as shown in Figure 4.9.61.



Figure 4.9.61. Image of 3D printed impeller made from 4047 aluminum

The impeller and support structure were cut from the build plate with EDM. After removal from the build plate, the impeller was fixtured such that the support structure could be removed from the impeller with the EDM. Images of the fixtured impeller, positioning in the EDM, and resultant cut are shown in Figure 62-Figure 4.9.64.

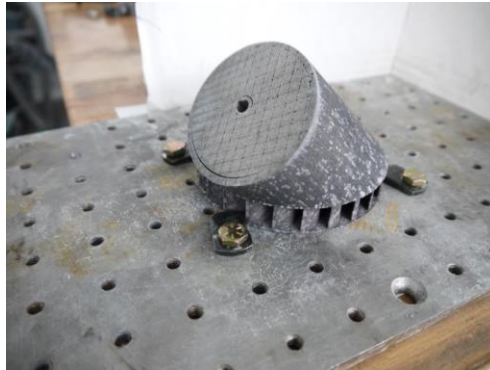


Figure 62. Fixtured impeller and support structure

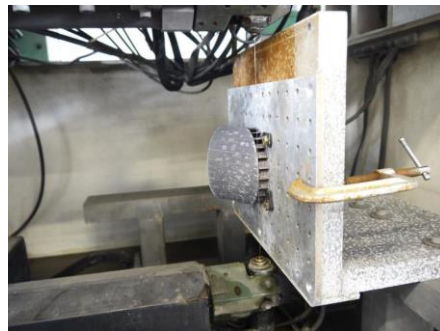


Figure 4.9.63. Impeller with support structure mounted in wire EDM

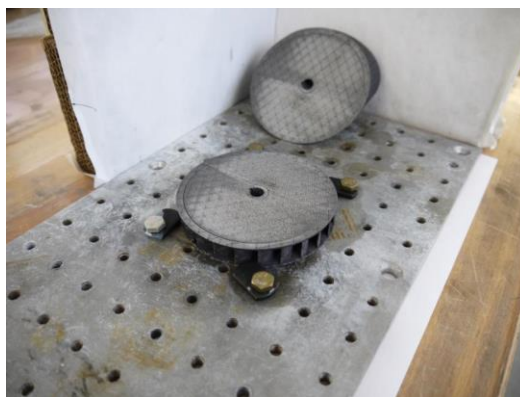


Figure 4.9.64. Impeller separated from main support structure after wire EDM

The impeller demo was carried out in the month of May. An evaluation criterion for the machined impellers was developed in order to determine the effectiveness of the GAM process. The purpose of the evaluations was to determine the effectiveness of the GAM process. As reported previously, 8 locations were probed, using the romer arm, around the lower surface and the upper machined surface, as shown in Figure 4.9.65. Care was taken to probe as closely as possible in the same (x, y) location on the lower surface and the upper machined surface.



Figure 4.9.65. Images of probing impeller with Romer arm

Metrolog software was used to collect the probing data and corresponding diameters were calculated by a least squares criterion, shown in Figure 4.9.66. The image also visually illustrates that the corresponding (x, y) coordinates of the points around the lower surface and the upper machined edge are very close to each other.

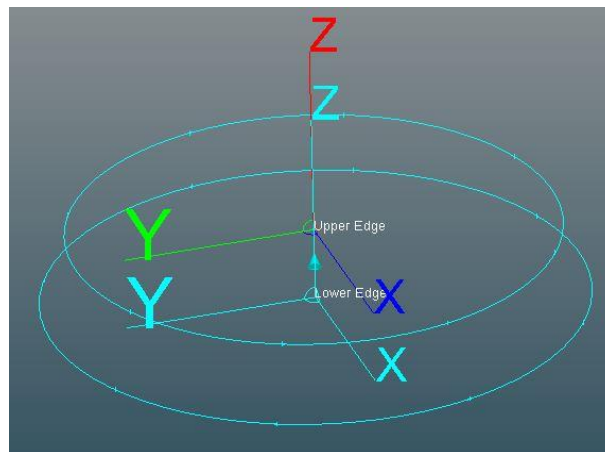


Figure 4.9.66. Image illustrating calculation of diameters from least squares

The lower edge of the impeller is the edge that was probed by the Renishaw probe on the HAAS mill in the CNC GAM process. Consequently, if the GAM app detects and responds to distortion, then the upper machined edge should exhibit a “morphed” shape that is similar to the lower edge. This probing strategy assumes that there is diametral distortion present on the lower edge of the impeller. If distortion is present on the lower edge, this evaluation should indicate if the GAM app is detecting and responding to the distortion. The analysis of the probing data is as follows:

- The radial location of each measured point on the lower edge and upper machined edge is compared to its respective least squares diameter value.

- If the GAM is detecting and responding to the distortion, the residuals of the points on the upper machined edge relative to its diameter should correlate to the residuals of the points on the lower edge relative to its diameter.

The results of the evaluations of the two machined impellers are shown below. For a high degree of correlation between lower edge and upper machined edge residuals, the values in red should be close zero and fairly uniform. This is because the “morphed” shape of the upper machined edge should match or correlate to the distortion of the lower edge, if it is present.

Impeller_1						
Lower Edge			Upper Machined Edge			Lower Residuals - Upper Residuals (mm)
Least Squares ϕ (mm)		97.520	Least Squares ϕ (mm)		88.062	
Measurements	Radial Data Points (mm)	Residuals (mm)	Measurements	Radial Data Points (mm)	Residuals (mm)	
1	48.664	0.096	1	43.976	0.055	0.042
2	48.843	-0.083	2	44.071	-0.040	-0.043
3	48.822	-0.062	3	44.079	-0.048	-0.014
4	48.674	0.086	4	43.966	0.065	0.021
5	48.694	0.066	5	44.018	0.013	0.053
6	48.863	-0.103	6	44.054	-0.023	-0.080
7	48.780	-0.020	7	44.066	-0.035	0.015
8	48.724	0.036	8	44.004	0.027	0.009

Impeller_2						
Lower Edge			Upper Machined Edge			Lower Residuals - Upper Residuals (mm)
Least Squares ϕ (mm)		97.188	Least Squares ϕ (mm)		88.022	
Measurements	Radial Data Points (mm)	Residuals (mm)	Measurements	Radial Data Points (mm)	Residuals (mm)	
1	48.662	-0.068	1	44.067	-0.056	-0.012
2	48.622	-0.028	2	44.069	-0.058	0.030
3	48.466	0.128	3	43.929	0.082	0.046
4	48.659	-0.065	4	43.974	0.037	-0.102
5	48.633	-0.039	5	44.094	-0.083	0.044
6	48.568	0.026	6	44.017	-0.006	0.032
7	48.576	0.018	7	43.977	0.034	-0.016
8	48.559	0.035	8	43.954	0.057	-0.022

The values in red (lower residuals minus upper machined residuals) show some non-uniformity and appear randomly distributed, which suggests a low degree of correlation, although that assessment is dependent upon what degree of accuracy is required of the GAM process. The low degree of correlation is likely because there was not significant diametral distortion present on the impellers.

Clamping Bracket (Simulated RIA)

A meeting was held with Dr. Dan Hanson and Edward Flinn at Rock Island Arsenal and a welded mast clamp assembly was identified as a potential use case. RIA indicated that the solid models of this part could not be shared with foreign nationals. In order to deal with this issue, we identified the critical features present on the part that the adaptive machining software algorithm would need to identify. We then created a solid model of an entirely new part that is geometrically and dimensionally different from the files provide to us. An image of the simulated mast clamp (clamping bracket) model is shown in Figure 4.9.67.

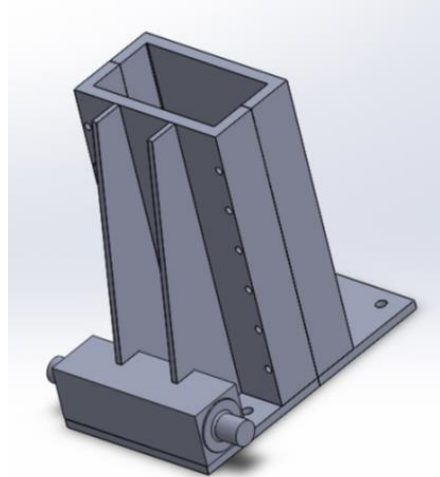


Figure 4.9.67. Image of solid model of clamping bracket

The deform function within SolidWorks was used to create simulated distortion that would be observed in the clamping bracket use case.. Images of the nominal and distorted clamping bracket are shown in Figure 4.9.68 and Figure 4.9.69, respectively.

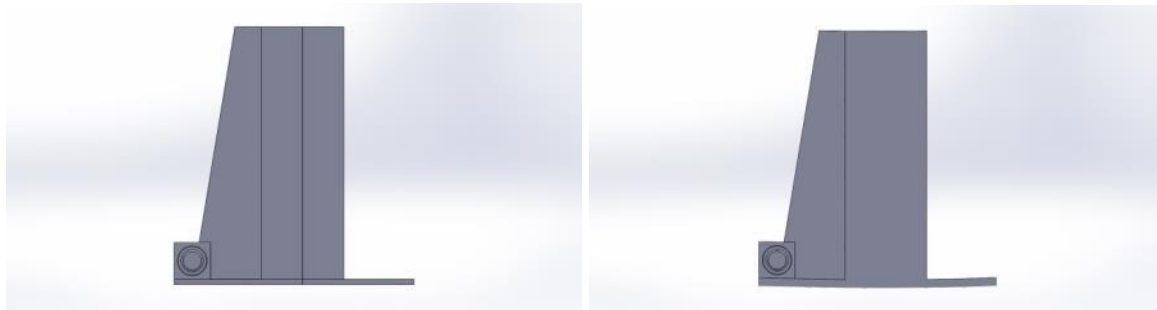


Figure 4.9.68. Nominal clamping bracket (left)

Figure 4.9.69. Distorted clamping bracket (right)

The clamping bracket is a weldment that often has issues with warping due to the welding process. Once acceptable parts were produced, work-holding methods for this particular part needed to be determined. A custom fixture was designed and machined manually out of aluminum stock. This custom fixture has been tested and deemed as a sufficient work-holding apparatus for probing and machining operations.

The CAD model for the clamping bracket was modified to reduce 3D metal printing costs, while maintaining the desired features for GAM as shown in Figure 4.9.70. The altered CAD model was truncated so that the entire height would not have to be 3D printed. Additionally, the cylindrical boss on one side was removed so that the clamping bracket could be placed in the fixture on its side. The raw, rectangular stock for cylindrical boss on the other side was left in place so that the cylindrical boss could be machined from the rectangular stock after the distortion in the base plate of the bracket was removed via machining.

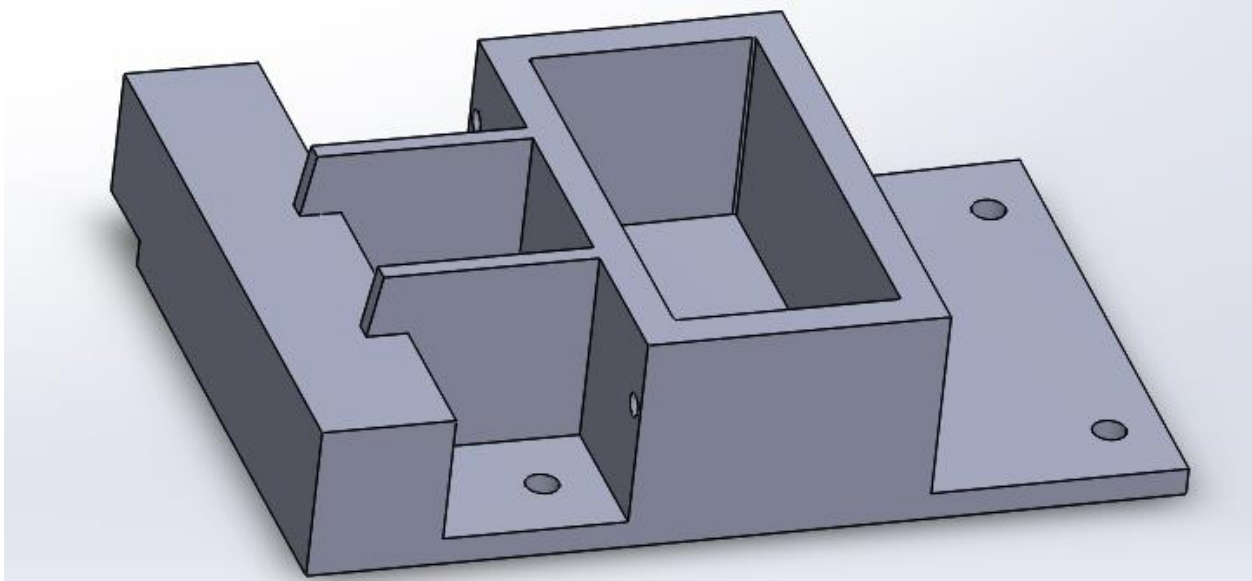


Figure 4.9.70. Image of truncated clamping bracket solid model

The truncated clamping bracket was 3D printed in stainless steel, as shown in Figure 4.9.71.

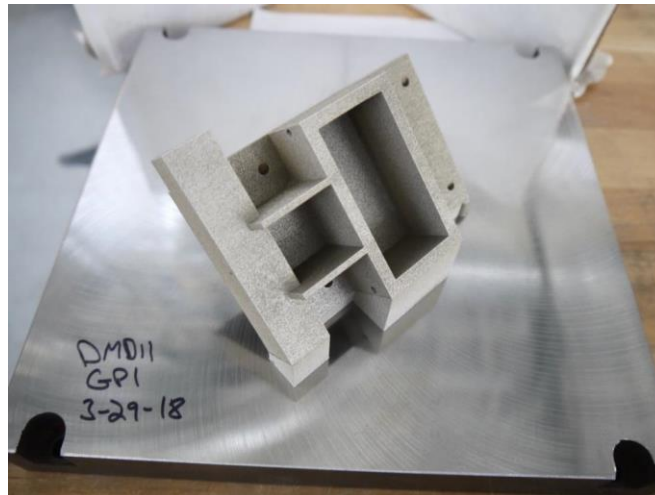


Figure 4.9.71. Image of truncated clamping bracket 3D printed in stainless steel

The GE team decided in the month of June that the GAM app would not be applied to the clamping bracket use case due to the fact that the GAM app, in its current condition, would not meet the requirements of the clamping bracket use case without considerable additional development of the GAM app. For purposes of documentation and explanation, a brief summary of the clamping bracket use case is given below. When the clamping bracket is fabricated, welding induced distortion is introduced into the flanges. Figure 4.9.72 shows the nominal clamping bracket with the minimum required flange thickness of 0.100" indicated, as well as the datum surface used for defining flatness. Figure 4.9.73 shows the distorted clamping bracket with the flange having extra material (0.150") to accommodate material removal to bring the distorted flange back into compliance with the flatness requirement.

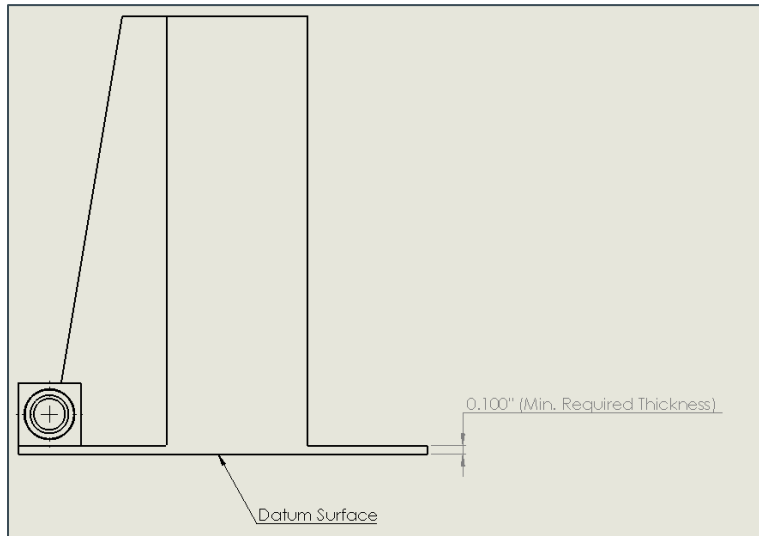


Figure 4.9.72. Image showing nominal clamping bracket with minimum required flange thickness

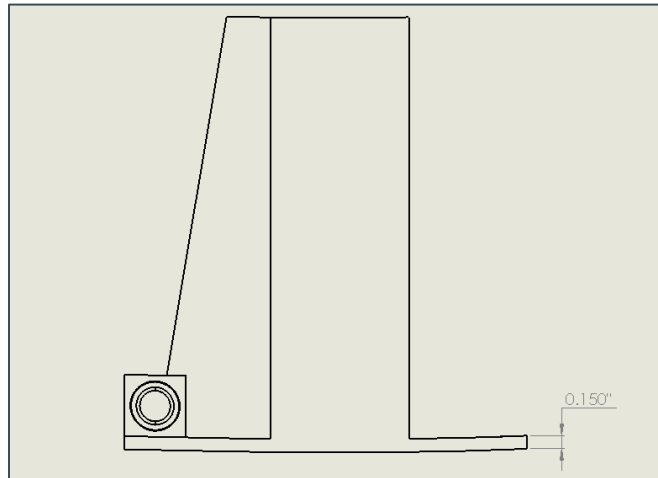


Figure 4.9.73. Image showing distorted clamping bracket with additional flange thickness

Figure 4.9.74 shows the distorted flange of the clamping bracket made flat with a milling operation, such that the thickness of the flange at the thinnest section is greater than or equal to 0.100". The image also shows the required distance between the datum surface of the flange of the center of the cylindrical feature milled onto the pivot bar (0.477"). The location of the cylindrical feature can float relative to the pivot bar in order to satisfy the 0.477" dimension.

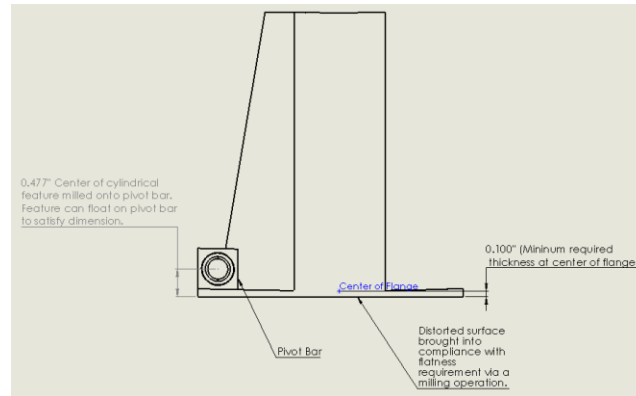


Figure 4.9.74. Image showing distorted flange of clamping bracket after milling operation

The GAM app was to be applied to this two-step milling operation, as follows:

1. Probe the distorted flange
2. Morph the cutting path which removes distortion via material removal
3. Offset the location of the cylindrical feature milled onto pivot bar to satisfy the 0.477" dimension.

The GE team decided that the GAM app could not be applied to the clamping bracket, as described above, without significant additional development of the app.

V INDUSTRY IMPACT & POTENTIAL

There are specific benefits to deploying the Geometric Adaptive Machining (GAM) solution that was developed under this program. As shown in the various use cases for the Rock Island Arsenal, where QCML leverages the GAM for CNC and GAM for robotic to improve machining of swivel links and large castings. The GAM technology will be key to RIA machining workflow as it will eliminate current manual processes, reduce scrap, and reduce machining time, which will result in \$MM in savings.

GE also has several applications that would benefit from adaptive machining technology in repair of gas turbine components. There are two primary benefits from these applications: 1) reduce the time to develop repairs, from 3 months to 1 week, and 2) reduce the required investment in plant and equipment from approximately \$1.25MM per application to \$200K by deploying adaptive machining on GE's Hass Machines. The same benefits also extend to an airfoil repair application for GE Aviation, which would enable insourcing of repair currently done outside the United States.

The geometric adaptive machining (GAM) solution will also benefit the broader U.S. manufacturing base. It would enable any machine tool to become adaptive with relatively low investment. The geometric adaptive nature of the solution would provide new capabilities in terms of machining composites, complex castings, and additively manufactured parts. Within GE, GAM has been successfully used to improve quality and minimize hand benching, an environmental health and safety consideration on the shop floor. GE also foresees that deploying geometric adaptive machining across the United States would help in-source tough repairs on complex components that currently either require a high cost replacement or are outsourced to locations where the cost is mitigated by lower labor cost. The net result would be savings to DoD and manufacturers, and increased U.S. manufacturing employment.

The plug-and-play approach will also have a huge impact on the penetration of this technology to SMEs. By eliminating the need for experts and reducing the time investment to develop new adaptive machining applications, this technology would be attractive for SMEs who require an agile approach for dealing with high-mix, low-volume production, or who perform operations—as described in the previous paragraph—that would benefit from geometric adaptive machining.

VI TECH TRANSITION PLAN & COMMERCIALIZATION

The toolkit is implemented in a modular format and modules can be chosen from the toolkit depending on the type of application for geometric adaptive machining. The toolkit will be available in three options.

1. GE stand-alone for CNC: this option enable GAM to be executed as a stand-alone module with user interface developed by GE
2. Metrolog CNC GAM: with this option, the GAM modules are integrated into Metrolog commercial software and executed from within Metrolog interface

GAM Category	Description	Software Modules	License	Total Cost
GE Stand-Alone CNC GAM	Stand alone application to perform adaptive machining on CNC machine tools	• Parasolid Geometric Kernel	\$15K	\$ 25K
		• AAT3D CappsNC	\$10K	
		• Probe Point Selection	~\$5K	
		• GE Morphing	~\$K	
Metrolog CNC GAM	Add-on to Metrolog inspection software to perform adaptive machining on CNC machine tools	• Metrolog offline inspection	\$30K	\$55K
		• Parasolid Geometric Kernel	\$15K	
		• AAT3D CappsNC	\$10K	
		• Probe Point Selection	~ \$5K	
		• GE Morphing	~ \$5K	
Metrolog Robotic GAM	Add-on to Metrolog inspection software to perform adaptive machining on robots	• Metrolog offline inspection + i-Robot	\$35K	\$60K
		• Parasolid Kernel	\$15K	
		• AAT3D CappsNC	\$10K	
		• Probe Point Selection	~ \$5	
		• GE Morphing	~ \$5	

Table 5.1.1. Toolkit modules and cost

VII WORKFORCE DEVELOPMENT

The deployment of geometric adaptive machining requires understanding of the various steps in the workflow. WIU-QCML work along with the team to document these steps and develop a training document that covers the set up and deployment of the adaptive machining toolkit. The training documents accompanying this report are:

- Probe Point Selection module
- Metrolog GAM workflow setup instructions
- AAT3D CappsNC Instructions
- Robotic GAM execution

VIII CONCLUSIONS/RECOMMENDATIONS

The used cases demonstrated in this program showed that the geometric adaptive machining toolkit technology can be used successfully develop and perform adaptive machining for machine tools and robotic applications. The plug-and-play hardware and software toolkit will enable legacy and modern machine tools and robots to perform adaptive machining. This approach to the technology will enable small and medium enterprises to perform geometric adaptive machining as part of their operations, which could impact their global competitiveness and stated.

Figure 8.1 show the baseline and current state of geometric adaptive machining toolkit solution. In this program the manual steps were automated and eliminating the highly expensive and time-consuming way of developing adaptive machining solution.

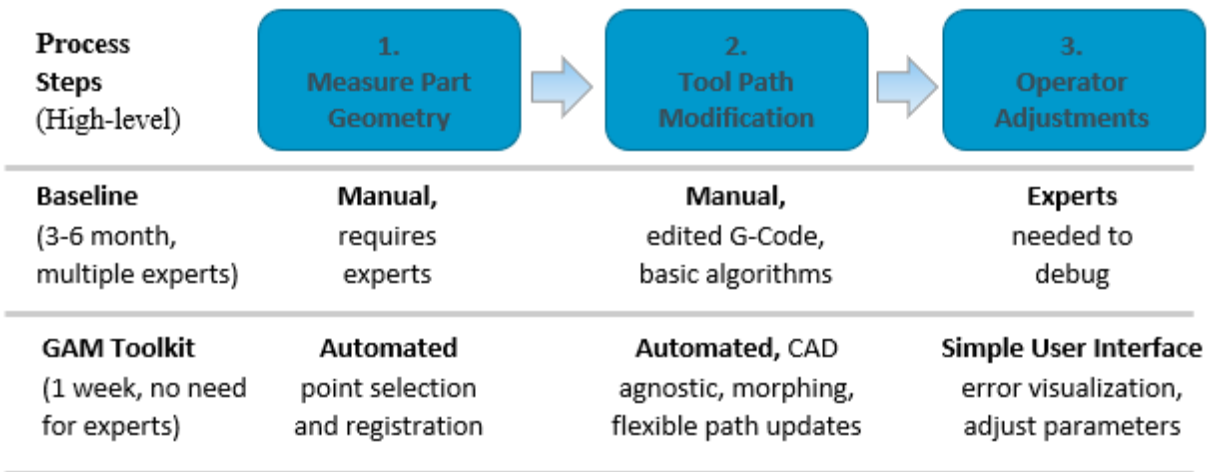


Figure 8.1. Project baseline & state of geometric adaptive machining toolkit

The results of the adaptive machining toolkit met the overall project goal of providing a portable, user friendly, commercially available toolkit that will reduce the development time for geometric-adaptive machining application. In addition, since the tool is designed to be retrofitted to low cost machine tools and robots the overall cost for implementing adaptive machining can be reduce by up to 80%.

IX LESSONS LEARNED

- **Probe points inspection:** the original scope of work was to use low cost Productivity Plus inspection module to convert DMIS program to g-code. After several months into the program, it was discovered that Productivity Plus does not have the capability. The team explore developing a module to do the conversion but, the time and resource was not available. AAT3D CaapNC was eventually adopted for converting DMIS to g-code
- **Toolpath morphing:** To generate the morph g-code, the initial plan was to adopt the strategy that GRC developed for its NX-based adaptive machining program. This strategy was to apply compensation to modify the nominal toolpath program known as the cutter location source file (CLS file). The modified CLS file is then imported back into the CAM software and then posted as g-code. We looked at two other CAM software HSMWorks and Mastercam to see if the strategy could be adopted seamlessly. Both software produces nominal toolpath like NX CLS, but the file formats are very different. Also, the modified CLS file could not be imported back into HSMWorks to be posted as morphed g-code. We therefore change the strategy by applying compensation to modify the nominal g-code directly. We developed Parasolid based morphing module to implement the morphing strategy

X DEFINITIONS

REFERENCES

1. Heckbert, P. S., and Garland, M., 1997. Survey of polygonal surface simplification algorithms. Tech. rep., CARNEGIE-MELLON UNIV PITTSBURGH PA SCHOOL OF COMPUTER SCIENCE.

2. Nadler, E., 1986. "Piecewise linear best l2 approximation on triangulations". *Approximation Theory V*, pp. 499–502.
3. Cohen-Steiner, D., Alliez, P., and Desbrun, M., 2004. "Variational shape approximation". In *ACM Transactions on Graphics (TOG)*, Vol. 23, ACM, pp. 905–914.
4. Cignoni, P., Rocchini, C., and Scopigno, R., 1998. "Metro: Measuring error on simplified surfaces". In *Computer Graphics Forum*, Vol. 17, Wiley Online Library, pp. 167–174.
5. Pauly, M., Gross, M., and Kobbelt, L. P., 2002. "Efficient simplification of point-sampled surfaces". In *Proceedings of the conference on Visualization'02*, IEEE Computer Society, pp. 163–170.
6. Luebke, D. P., 2001. "A developer's survey of polygonal simplification algorithms". *IEEE Computer Graphics and Applications*, 21(3), pp. 24–35.
7. Garland, M., 1999. "Multiresolution modeling: Survey & future opportunities". *State of the art report*, pp. 111–131.
8. Quinn, J. A., Langbein, F. C., and Martin, R. R., 2007. "Low-discrepancy point sampling of meshes for rendering." In *SPBG*, pp. 19–28.
9. Shirley, P., et al., 1991. "Discrepancy as a quality measure for sample distributions". In *Proc. Eurographics*, Vol. 91, pp. 183–194.
10. Rodolà, E., Albarelli, A., Cremers, D., and Torsello, A., 2015. "A simple and effective relevance-based point sampling for 3d shapes". *Pattern Recognition Letters*, 59, pp. 41–47.
11. Alexa, M., Rusinkiewicz, S., Nehab, D., and Shilane, P., 2004. "Stratified point sampling of 3d models". In *Proc. Eurographics Symp. on Point-Based Graphics*, pp. 49–56.
12. Oudot, S., and Boissonnat, J.-D., 2003. "Provably good surface sampling and approximation." In *Symposium on Geometry Processing*, pp. 9–18.
13. Boissonnat, J.-D., and Oudot, S., 2005. "Provably good sampling and meshing of surfaces". *Graphical Models*, 67(5), pp. 405–451.
14. Das, G., and Goodrich, M. T., 1995. "On the complexity of approximating and illuminating three-dimensional convex polyhedra". In *Workshop on Algorithms and Data Structures*, Springer, pp. 74–85.
15. Brönnimann, H., and Goodrich, M. T., 1995. "Almost optimal set covers in finite vc-dimension". *Discrete & Computational Geometry*, 14(4), pp. 463–479.
16. Obeidat, S. M., and Raman, S., 2009. "An intelligent sampling method for inspecting free-form surfaces". *The International Journal of Advanced Manufacturing Technology*, 40(11), pp. 1125–1136.
17.] Lai, J., Fu, J., Shen, H., Gan, W., and Chen, Z., 2015. "Machining error inspection of t-spline surface by on-machine measurement". *International Journal of Precision Engineering and Manufacturing*, 16(3), pp. 433–439.
18. ElKott, D. F., and Veldhuis, S. C., 2007. "Cad-based sampling for cmm inspection of models with sculptured features". *Engineering with computers*, 23(3), pp. 187–206.

19. Yu, M., Zhang, Y., Li, Y., and Zhang, D., 2013. "Adaptive sampling method for inspection planning on cmm for free-form surfaces". *The International Journal of Advanced Manufacturing Technology*, 67(9-12), pp. 1967–1975.
20. Vezzetti, E., 2009. "Adaptive sampling plan design methodology for reverse engineering acquisition". *The International Journal of Advanced Manufacturing Technology*, 42(7), pp. 780–792.
21. Brus, D. J., and Heuvelink, G. B., 2007. "Optimization of sample patterns for universal kriging of environmental variables". *Geoderma*, 138(1-2), pp. 86–95.
22. Müller, W. G., 2007. *Collecting spatial data: optimum design of experiments for random fields*. Springer Science & Business Media.
23. Hengl, T., Heuvelink, G. B., and Stein, A., 2004. "A generic framework for spatial prediction of soil variables based on regression-kriging". *Geoderma*, 120(1-2), pp. 75–93.
24. Lesch, S., 2005. "Sensor-directed response surface sampling designs for characterizing spatial variation in soil properties". *Computers and Electronics in Agriculture*, 46(1-3), pp. 153–179.
25. Hengl, T., Rossiter, D. G., and Stein, A., 2003. "Soil sampling strategies for spatial prediction by correlation with auxiliary maps". *Soil Research*, 41(8), pp. 1403–1422.
26. Huang, Y., and Qian, X., 2007. "Dynamic b-spline surface reconstruction: Closing the sensing-and-modeling loop in 3d digitization". *Computer-Aided Design*, 39(11), pp. 987–1002.
27. Advanced Manufacturing Propulsion Initiative (AMPI) Call 14, Contract FA865012C5300, "Adaptive Composites Machining"
28. Rangarajan, Arvind, et al. "System and method for adaptive machining." U.S. Patent No. 8,578,579. 12 Nov. 2013.
29. http://www.innovmetric.com/sites/default/files/documents/pw_products_letter_eng_web_1.pdf
30. <http://www.rapidform.com/products/xos/overview/>
31. <http://geaviationservicesolutions.com/lib/pdfs/v07i05.pdf>
32. B. K. P. Horn, "Close-form solution of absolute orientation using unit quaternions," *J. Opt. Soc. Am. A*, vol. 4, no. 4, pp.629 -642 1987
33. Qian, X., Harding, K.G., "Partitioning positional and normal space for fast occlusion detection," *ASME 2003 International Design Engineering Technical Conferences and Computers and Information in Engineering Conference*, 737-744.
34. Huang, Y., Qian, X., "Dynamic B-spline surface reconstruction: Closing the sensing-and-modeling loop in 3D digitization," *Computer-Aided Design*, 2007, 39 (11), 987-1002.
35. Huang, Y., Qian, X., "A dynamic sensing-and-modeling approach to three-dimensional point-and area-sensor integration," *ASME Journal of manufacturing science and engineering*, 2007, 129 (3), 623-635.
36. Huang, Y., Qian, X., "An efficient sensing localization algorithm for free-form surface digitization," *ASME Journal of Computing and Information Science in Engineering*, 2008, 8 (2), 021008.
37. Graham, M., Jackson, J., "System and method for numerical control processing of an in-processing part." U.S. Patent No. 6,256,546. 3 Jul. 2001.

38. Lee, S., Wolberg, G., Shin, S. Y., "Scattered Data Interpolation with Multilevel B-splines," IEEE Trans. on Visualization and Computer Graphics, Vol. 3, No. 3, pp. 228-244, July-September 1997.
39. Yang, P., Qian, X., "Multi-level B-spline Approach to Object Modeling with Scatted Data Points," Technical Report, Illinois Institute of Technology, 2007.
40. Piegl, L., Tiller, W., The NURBS Book, second edition, Springer-Verlag, New York, 1997.
41. "Interactive Work Instructions (IWI)", finalist in MTConnect Challenge, 2014:
<http://ncdmm.org/mtconnect-challenge/>.
42. Qian, X., Harding, K.G., "Computational approach for optimal sensor setup," SPIE Optical Engineering, 42 (5), 1238-1248.

XI APPENDICES

Software Source Codes and Executables

1. PointSampling
2. pointSamplingUI (UI to execute point sampling application)
3. gamUI (UI to execute stand-alone GAM)
4. parasolidBestfit (Horn's 3D Bestfit)
5. parseMetrologData (parse input/output data for Metrolog)
6. probePointsParser (parse measured probe points data)
7. probePointsParserUI (user interface application for probePointParser module)
8. MultilevelBsplne_commandLine.exe (non-rigid body transformation)
9. morphToolpathProgram (modify g-code)

Training Guide/User Manual

1. AAT3D_CappsNC_Instructions
2. Metrolog Setup Workflow
3. Point sampling application user guide

Validation/Testing

- Point cloud selection for touch probing
- Robotic Adaptive Torch Cutting Time Study